TÜBİTAK

Turkish Journal of Earth Sciences

http://journals.tubitak.gov.tr/earth/

Research Article

Turkish J Earth Sci
(2021) 30: 862-881

doi:10.3906/yer-2107-28

Fault-controlled gas escapes in the shelf sediments of the Saros Gulf, NE Aegean Sea

Şebnem ÖNDER[1,*], Naci GÖRÜR[2], Alina POLONIA[3], Luca GASPERINI[3]

[1]Department of Geophysical Engineering, Faculty of Engineering, Çanakkale Onsekiz Mart University, Çanakkale, Turkey

[2]The Science Academy, İstanbul, Turkey

[3]Institute of Marine Sciences, National Research Council, Bologna, Italy

Received: 29.07.2021 • **Accepted/Published Online:** 06.10.2021 • **Final Version:** 30.10.2021

Abstract: High-resolution marine seismic reflection studies on the eastern shelf of the Saros Gulf have revealed the presence of gas-charged sediments across a narrow submarine valley incised by the Ganos Fault along the North Anatolian Fault system. Quaternary sediments, accumulated during glacial and interglacial periods through transgressional and progradational units, were controlled by glacio-eustatic sea-level fluctuations and tectonic deformation. The transgressional units made of upward-fining deposits created seals at their tops to form gas accumulation pockets. Conversely, the progradational units appear heavily eroded at their top, which is unfavorable for gas accumulation. The sediment's gas accumulation features include enhanced reflections, acoustic blanking (or blanket), acoustic turbidity, acoustic curtain, and acoustic columns. In contrast, the gas escape features consist of acoustic plumes, cloudy turbidity, domes, and pockmarks. Their concentration along the Ganos Fault indicates that active deformation, punctuated by large magnitude earthquakes, has played an essential role in their formation, storage, and seep. Understanding these interactions may provide valuable contributions to hydrocarbon explorations and early-warning strategies against earthquake risk.

Key words: Aegean Sea, North Anatolian Fault, Gulf of Saros, seismic stratigraphy, high-resolution seismic reflection, gas seeps

1. Introduction

The Saros Gulf, in the NE Aegean Sea (Figure 1a), is a triangular-shaped topographic depression formed along the North Anatolian Fault (NAF) principal displacement zone.

A densely spaced grid of high-resolution marine seismic reflection profiles collected in the eastern shelf of the gulf was employed to reconstruct shallow-stratigraphy and morphobathymetry, and the presence of tectonic deformation affecting the uppermost sedimentary sequence. Seismic profiles image extensive gas accumulation and diffused seepage features. Understanding this system and how active tectonics controls gas escapes in the Saros shelf is important for two main reasons: 1) It may provide valuable contributions to hydrocarbon explorations in shallow-water environments, and 2) It is the first step to study relationships between gas and fluids emission from the seafloor and seismic activity. The aim of this work is, therefore, twofold. First, we describe, map, and interpret all the gas-related features in the study area by using available marine geophysical data. Second, after analyzing seismic stratigraphy and the presence of active or inactivated faults, we discuss possible mechanisms bringing deep-seated thermogenic gas up to the shallow depths where it could mix with a biogenic component and how and where it seeps at the seafloor and the water column.

1.1. Geodynamic Setting

The Saros Gulf, in northwestern Anatolia, forms where two different tectonic regimes have interfered since the middle Miocene (Figure 1b). They are the N-S extensional and NE-SW dextral strike-slip regimes, variably interacting to form a complex suite of tectonic structures, including the depression corresponding to the Saros Gulf basin. The causes and timing of the N-S extensional regime are debated. Hypotheses include i) extension to the westward escape of Anatolian Plate, in response to the Miocene collision between the African and the Eurasian Plates along the Bitlis-Zagros Suture Zone (Dewey and Şengör, 1979; Şengör, 1982; Şengör et al., 1985; Taymaz et al., 1991); ii) back-arc spreading resulting from the subduction of the African Plate beneath the Anatolian Plate along the Hellenic-Cyprus arc (Berckhemer, 1977; Le Pichon and Angelier, 1981); iii) gravitational spreading of the Aegean crust, which had been thickened in the Eocene, owing to the closure of the Northern Branches of the Neo-Tethyan

* Correspondence: selbek@comu.edu.tr

Ocean (Le Pichon and Angelier, 1979; Seyitoğlu and Scott, 1991).

The NE-SW dextral strike-slip tectonic regime in the Marmara region (Figure 1b) is related to the NAF emplacement, which developed as a result of the Anatolia tectonic escape since middle Miocene times (Şengör et al., 2005; Görür and Elbek, 2013). From the earliest phases to the present, its evolution in the Marmara region followed the structural stages described by Tchalenko (1970) and Hatem et al. (2017). The most prominent expression of the NE-SW right-lateral strike-slip deformation in the region is the Ganos Fault, formed in the early Pliocene as P-shears of the post-peak structure stage.

1.2. Basin formation

The opening of the Saros Gulf has been the subject of discussion for a long time. Various hypotheses were put forward to explain its formation, including an extensional graben (i.e., Saner, 1985; Şengör et al., 1985; Taymaz et al., 1991; Çağatay et al., 1998), a negative flower structure (Kurt et al. 2000), and a pull-apart basin (Tüysüz et al. 1998). According to the graben model, the NAF reached this area before the late Pliocene, with an original concave southward curvature, and then splits into several NE-SW strands in the vicinity of the Sea of Marmara. One of these strands, the Ganos Fault, is still active and forms the southern margin of the Saros Gulf. Continuous N-S

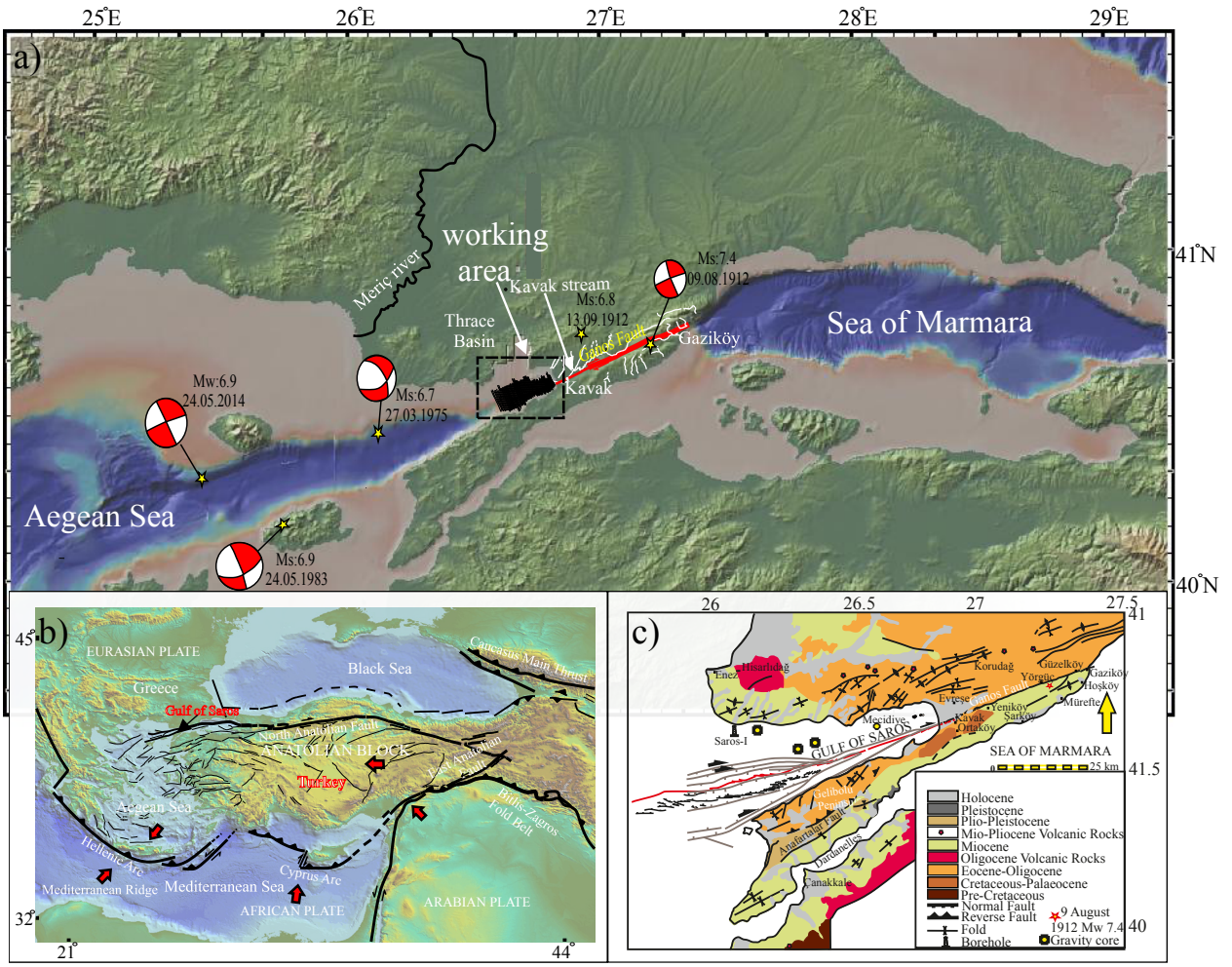

Figure 1. a) The Saros Gulf in the North Aegean Sea. Black lines indicate position of Chirp and Sparker profiles collected during the 2005 and 2011 cruises onboard R/V Urania. The base maps were prepared using the GeoMapApp (http://www.geomapapp.org/). Focal mechanisms of Ms≥ 6 earthquakes are shown by red beach balls (KOERI[1], Konca et al., 2018b and Aksoy, 2021). Tectonic framework of Anatolia and surroundings compiled from Jarvis et. al., 2008 and Yolsal-Çevikbilen and Taymaz, 2012; (Image credit ETOPOI Global Relief Amante and Eakins,2009). c) Geological map of Gulf of Saros modified from Çağatay et al. (1998), Emre et al. (2013), Kurt et al. (2000), and Aksoy et al. (2010).

[1] KOERI (2021). Earthquake Catalogue of Regional Earthquake Tsunami Monitoring Center [online]. Website http://www.koeri.boun.edu.tr/sismo/2/earthquake-catalog/ [01 July 2021].

stretching accentuated the original curvature of the NAF in the Marmara region and led to the formation of southward migrating new strands, including the narrow NE-SW-oriented Saros Gulf (Şengör et al., 1985; Çağatay et. al., 1998). In this model, two points need to be discussed, the first of which concerns the onset of the NAF in the Saros Gulf. Recent studies indicate that the present-day NAF could be a relatively young feature that did not reach the Marmara region earlier than 200 kyr ago (Şengör et al. 2005; Görür and Elbek, 2013). In this case, the formation of the Saros Gulf should pre-date the NAF emplacement. The second point concerns the position of the Ganos Fault in the Gulf of Saros. Differing from past reconstructions, recent works, based on high-resolution marine geophysical data (Alpar and Yaltırak, 2002; Gasperini et al., 2013 and 2018), have shown that the Ganos Fault lies in the gulf along the toe of the northern shelf rather than forming the north scarp of the southern shelf.

In summary, we could assume that the Saros Gulf underwent the effects of both forearc extension and strike-slip tectonic regimes, whose effects were variable in time and space, and created a variety of structures with complex overprinting patterns (Görür and Okay, 1996; Görür and Elbek, 2013). While the extensional structures constituted the stratigraphic basement of the gulf, subsequent deposits appear mainly affected by strike-slip deformation. The forearc tectonic regime has also driven the formation of the depression corresponding to the Thrace Basin, terminated in the Oligocene, and subsequently uplifted and eroded. In middle/late Miocene, the Thrace Basin was affected by a pervasive and shallower dextral shear deformation, which might correspond to the emplacement of the westernmost NAF shear zone. This shear system splays in the Saros Gulf, forming a dense damage zone, including normal and strike-slip faults (Davatzes and Aydın, 2003; Myers and Aydın, 2004), probably enhancing fault zone permeability, with significant impact on fluid flow.

1.3. Structural geology

A geological map of the Saros Gulf is shown in Figure 1c. NE-SW-oriented faults and folds are the dominant tectonic structures, the former mostly belonging to the various splays of the Ganos Fault. Folds are broad and north plunging and appear as discontinuous features with wavelengths of about 2 km and amplitudes of 200 m (Figure 1c). They are mostly symmetrical, but around the Ganos Fault and the Hisarlıdağ-Korudağ relief, they seem asymmetric, tight, sometimes overturned (Tüysüz et al.,1998; Görür and Elbek, 2013). Folds occur in Eocene to Oligocene and Miocene sediments (Figure 1c) and belong to the forearc palaeotectonic regime of the Thrace basin, whereas the Miocene folds are mostly related to the NAF (Görür and Okay, 1996; Şengör et al., 2005; Görür and Elbek, 2013).

1.4. Stratigraphy

The Saros Gulf formed starting from the late Pliocene, and therefore all rocks older than this age are considered the stratigraphic basement. The presence of an erosional unconformity between the basement and overlying Quaternary sediments on the shelf indicates that in late Pliocene times the shelf was either a non-depositional or erosional environment (Çağatay et al., 1998). The Saros Gulf basement crops out at both north and south margins and is mainly characterized by Miocene fluvio-lacustrine and shallow-marine sediments, consisting of conglomerates, sandstones, and shales, with ostracoda and mammal's fossils (Figure 1c). They interfinger in part with shallow-marine oolithic limestone, sandstone, and claystone, rich in Mactra fossils (Gazhanedere, Kirazlı, Alçıtepe Formations) (Sümengen et al., 1987; Siyako, 1989; Yaltırak, 1995).

Basement rocks are overlain on land by upper Pliocene to Quaternary sediments through an angular unconformity. The upper Pliocene sediments mostly occur in the Gallipoli Peninsula, where it comprises 350 m-thick reddish-brown conglomerate, sandstone, and shale, in part with coal seams, belonging to the so-called Conkbayırı Formation (Figure 1c) (Saner, 1985; Yaltırak, 1995) This clastic succession has an unconformable contact with the underlying formations. It displays an upward-coarsening sequence with many channel features, indicating that it generally formed in a fluvio-deltaic environment. The onshore Quaternary sediments crop out along the coastal areas and are mainly represented by Ostrea-rich conglomerates and sandstones (Marmara Formation), forming well-developed marine terraces (Sümengen et al., 1987; Siyako et al., 1989; Yaltırak, 1995).

2. Methods

We used high-resolution multibeam bathymetric and seismic reflection data collected during the Cruise MARM11 carried out on board R/V Urania in 2011. The vessel was equipped with DGPS and SEAPATH positioning system (satellite link by FUGRO), single-beam and multibeam bathymetry, and integrated geophysical and oceanographical data acquisition systems (ADCP, Chirp SBP, Sparker etc.).

Bathymetric data were collected by using Konsberg-Simrad EM-3000 and Reson 8160 multibeam systems. Multibeam data uncertainties are generally depth-dependent and over 5 m in the study area. Chirp data were collected with a 16 transducer Benthos Chirp II subbottom system. Sparker data were obtained using a 1.5 KJ multi-tip sparker GEO-SOURCES system and a single-channel, analog, 10 m-long streamer. Digitalization was performed using the SwanPro software (Communication Technology, Cesena, Italy). Sparker and Chirp data were processed and

interpreted at ISMAR-CNR in Bologna using SeisPrho (Gasperini and Stanghellini, 2009) and the Kingdom Suite Software, 2015 version.

3. Results

3.1. Structural setting

A newly-compiled, high-resolution multibeam morpho-bathymetric map of the Saros Gulf (Figure 2) enabled us to add new details on available tectonic models. First, we note that the present-day incipient deformation belt connecting the Ganos Fault to the offshore region appears very focused and narrow. This fault zone lies onshore between Gaziköy and Kavak and enters the gulf along with a narrow, NE-SW-trending and westward-deepening valley (from now on, incised valley). The incised valley extends for about 40 km and connects the eastern edge of the gulf with the 800 m deep basin towards the west (Figure 2). The northern slope of the valley is represented by a linear and vertical scarp, whereas the southern flank shows a relatively smooth morphology. The incised valley lays along the submarine continuation of the Ganos Fault, i.e., the NAF principal displacement zone (Figures 2, 3, and 4). However, the seismic reflection grid analysis enabled us to identify a more complex fault network that has a poor topographic expression at the seafloor.

The morphostructural map of Figure 3 shows groups of faults developed during different phases. The first group cuts the basement and the Quaternary shelf sediments but barely reaches up to the seabed; it forms a wide deformation zone on both flanks of the incised valley (Figure 3). The second group cuts the seabed in the closest incised valley surroundings representing the incipient deformation pattern (Figure 3).

The Saros Gulf's edges are bounded by the dextral strike-slip splays of the Ganos Fault, which mostly show dip-slip components (oblique faults), although *en echelon* normal faults are also observed (Figures 1c and 3). In the northern margin, the deformation appears more diffuse, with oblique faults dipping towards the south. In contrast, in the southern margin, there are multiple structures down throwing to the north, giving an asymmetrical graben geometry to the gulf. Dip angles of the northern oblique faults are commonly lower than those of the southern ones. Most of the oblique faults seem to be active as they cut the seafloor. However, many of them in the northern shelf seem inactive as they are covered by Quaternary sediments (Figures 5-9).

3.2. Seismostratigraphy

Based on analysis of both Chirp-sonar and Sparker seismic reflection profiles, the Quaternary sediments, ranging in thickness from 0 to 90 m (Figure 4), are divided into three seismostratigraphic units correlated to the Quaternary deposits described by Çağatay et al. (1998). Seismic units display characteristic facies and are separated by clear unconformities and correlative conformities that will be described from the basement to the seafloor using Sparker (SP) and Chirp (CH) profiles. Since we interpreted travel-time sections, thickness estimates were carried out assuming a constant 1500 m/s sound velocity.

3.2.1. Unit-3

It constitutes the basal part of the Quaternary succession and overlies the basement rocks above an erosional

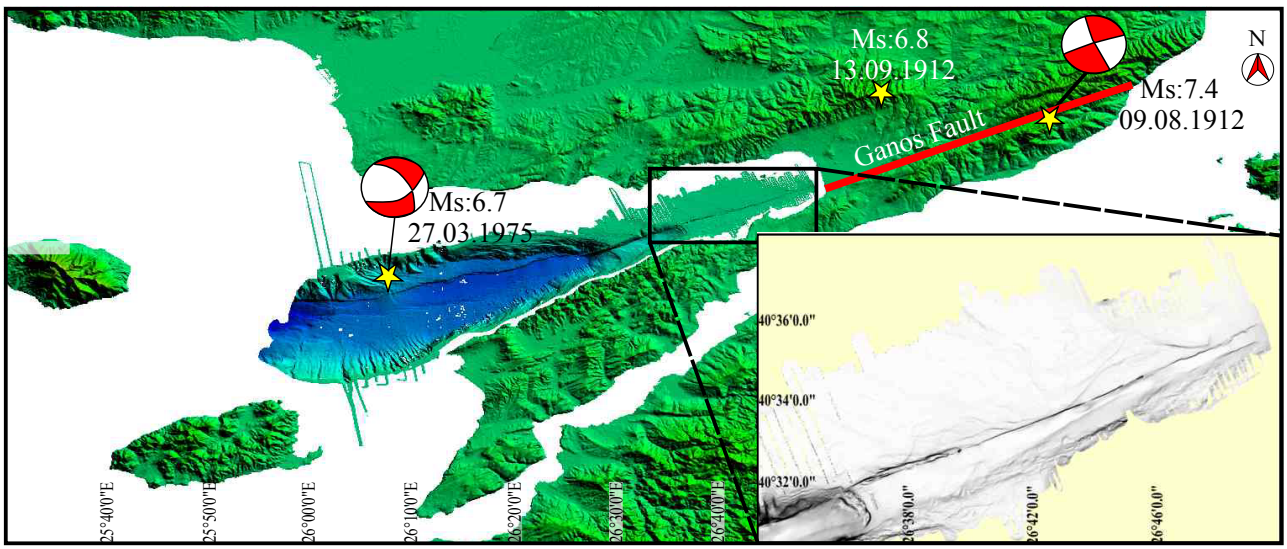

Figure 2. Multibeam bathymetric map of the Gulf of Saros (from RV Urania 2005 and 2011 cruises). Topography data downloaded from NOAA National Geophysical Data Center ETOPOI Global Relief (Amante and Eakins,2009). Focal mechanism of destructive earthquakes (Ms≥ 6) since 1900 are shown by red beach balls from KOERI and Aksoy, 2021.

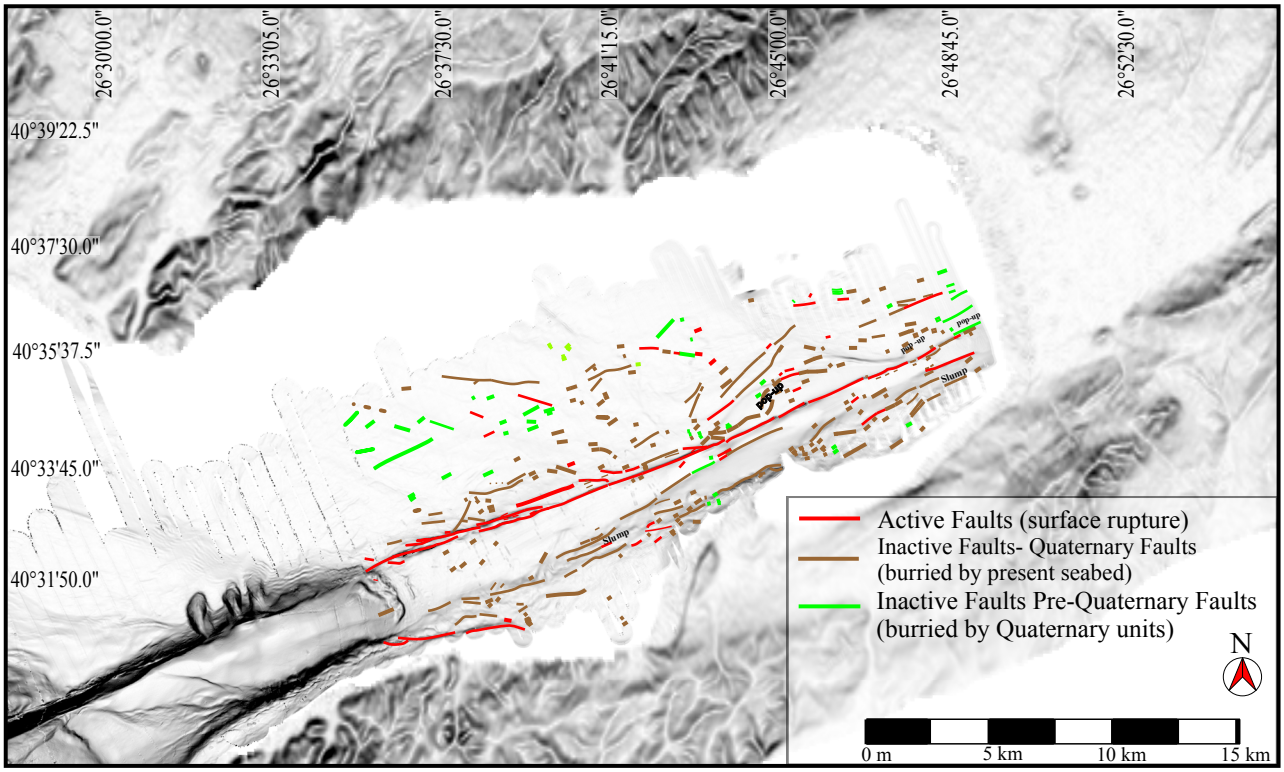

Figure 3. Morphostructural map of the Gulf of Saros with indicated active (red lines) and inactive (brown and green lines) fault traces. Bathymetry (slope map) from R/V Urania 2005 and 2011 cruises; topography from NOAA National Geophysical Data Center ETOPOI Global Relief (Amante and Eakins, 2009).

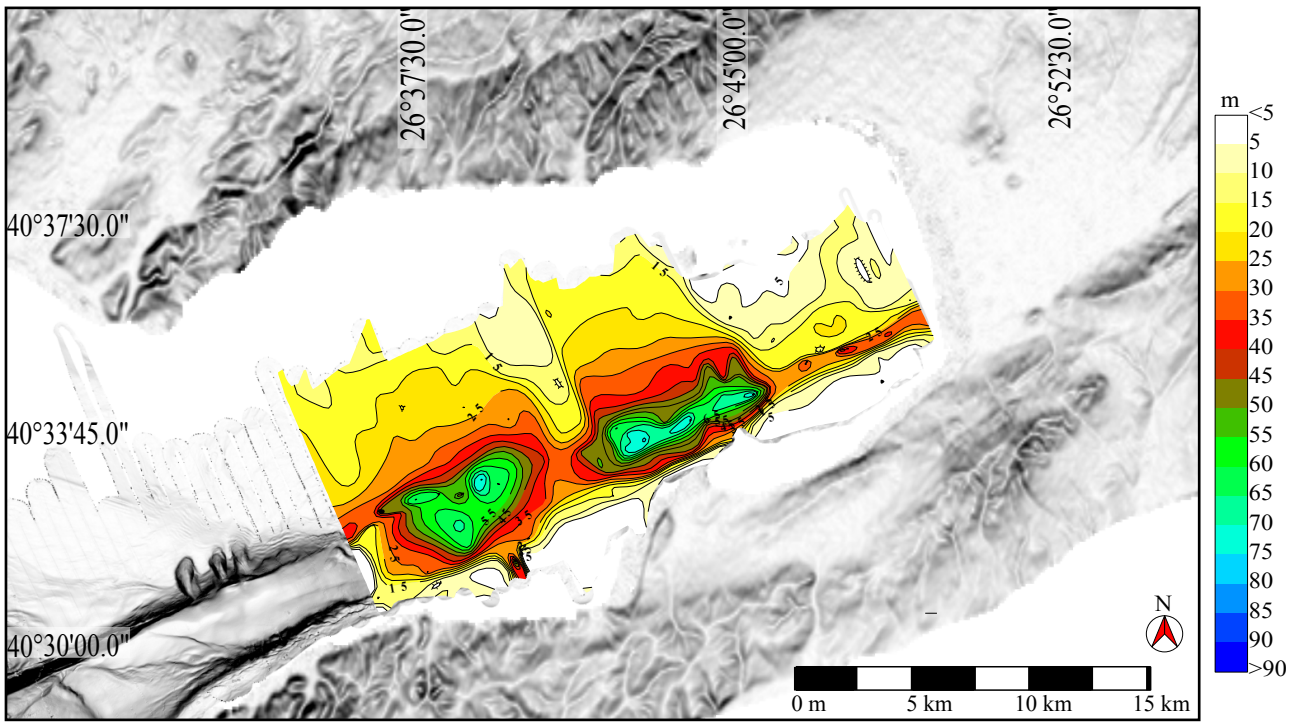

Figure 4. Isopach map displaying total sediment thickness of Quaternary sediments. Bathymetry (slope map) from R/V Urania 2005 and 2011 cruises; topography from NOAA National Geophysical Data Center ETOPOI Global Relief (Amante and Eakins, 2009).

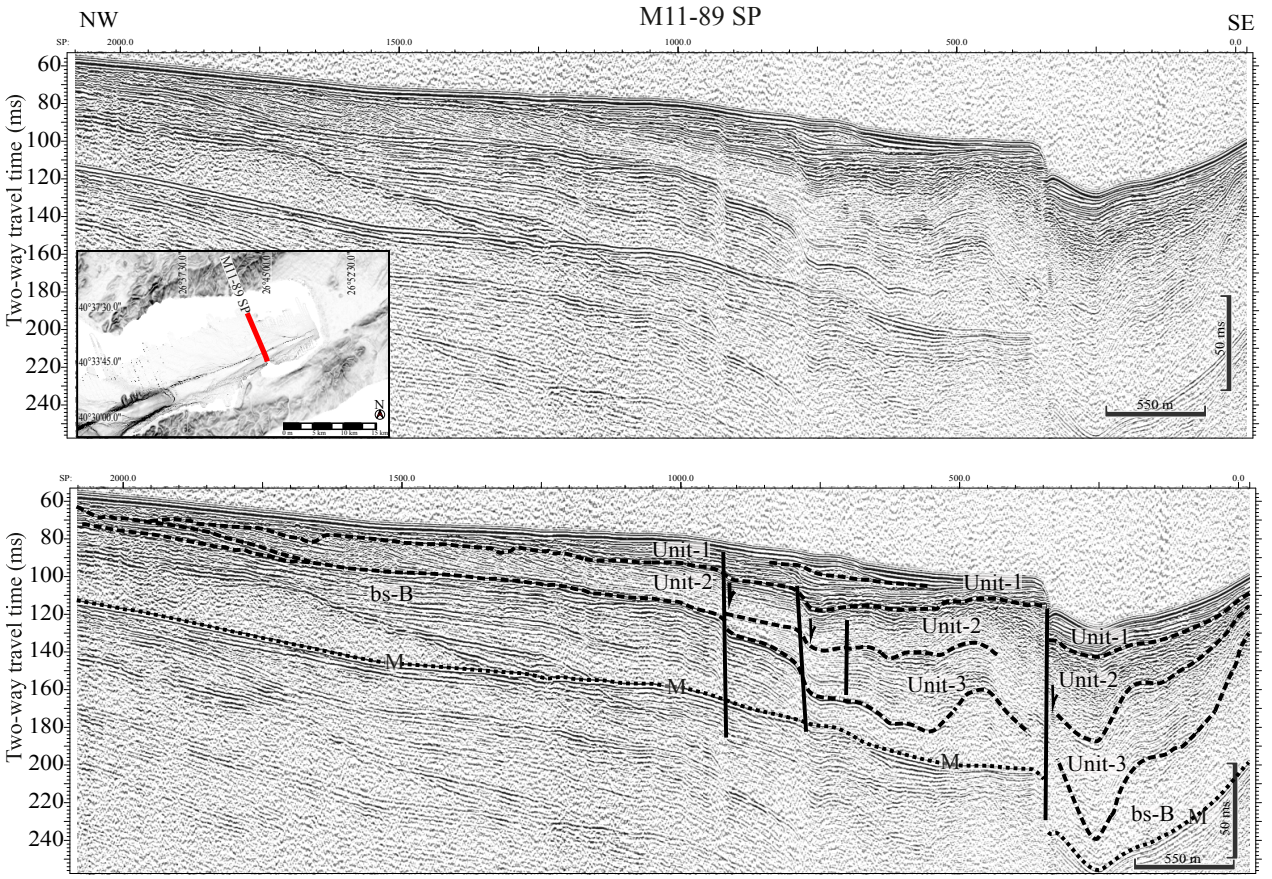

Figure 5. Sparker profile M11-89 (top) and its interpretation (bottom) showing main tectonic features and seismic sequences Unit-1 to Unit-3; bs-B basement, M multiple. Location in the inset.

unconformity (Figures 5–15). It is formed by parallel to subparallel, continuous to semicontinuous, high amplitude, and moderate- to high-frequency internal reflectors. It is generally 4 to 53 m thick on the shelf, but it seems to thicken towards the south and southeast, i.e. towards the basin and the incised valley of the Ganos Fault. We interpret this unit as deposited during a transgressive phase, and its characteristic reflectors and stratigraphic position indicate that it can be correlated with the Ostrea-rich conglomerates and sandstones of the Marmara Formation. Electron-spin resonance dating, and its fossil content suggest that the Marmara Formation is of Milazzian to Tyrrhenian age, which corresponds to the Isotope Stage-5 (MIS-5) (Shackleton and Opdyke, 1989; Erol and Çetin, 1995; Yaltırak, 1996; Çağatay et al., 1998; Eriş, 2007; Görür and Çağatay, 2010); therefore, Unit-3 should have deposited between 129 and 78 ka.

3.2.2. Unit-2

Unit-2 unconformably overlies Unit-3 and shows low-angle seaward prograding clinoforms, semicontinuous to discontinuous, contorted to chaotic facies, and low amplitude internal reflectors (Figures 5–10, 13–19). The chaotic facies become more apparent in this sequence around the incised valley. Along the profile M11- 71 SP, high amplitude internal reflectors are also visible (Figure 8). In profile M11-115 SP, the high amplitude parallel reflectors occur in the upper part of the sequence above the chaotic facies, forming topsets (Figure 6). Overall, Unit-2 constitutes a basinward thickening body. In profile M11-116 SP, Unit-2 is absent in the NW part of the section but progressively thickens up to 17 m towards the SE (Figure 7). The upper part of this sequence was cored and dated on the northern shelf of the Saros Gulf and consists of pebbly and shelly sand and mud, ranging in age from 16 to 11 ka (Çağatay et al., 1998). The presence of clinoforms and the peculiar seismic texture of Unit-2 suggest that it was deposited as a prograding deltaic succession during a sea-level lowstand, probably during marine Isotope Stage-2 (MIS-2) (Shackleton and Opdyke, 73).

3.2.3. Unit-1

Unit-1 represents the top of the Quaternary succession and drapes in places that are all older units, including the basement rocks. It is up to 48 m thick and consists of two subunits with different seismic facies (Figure 11). The lower

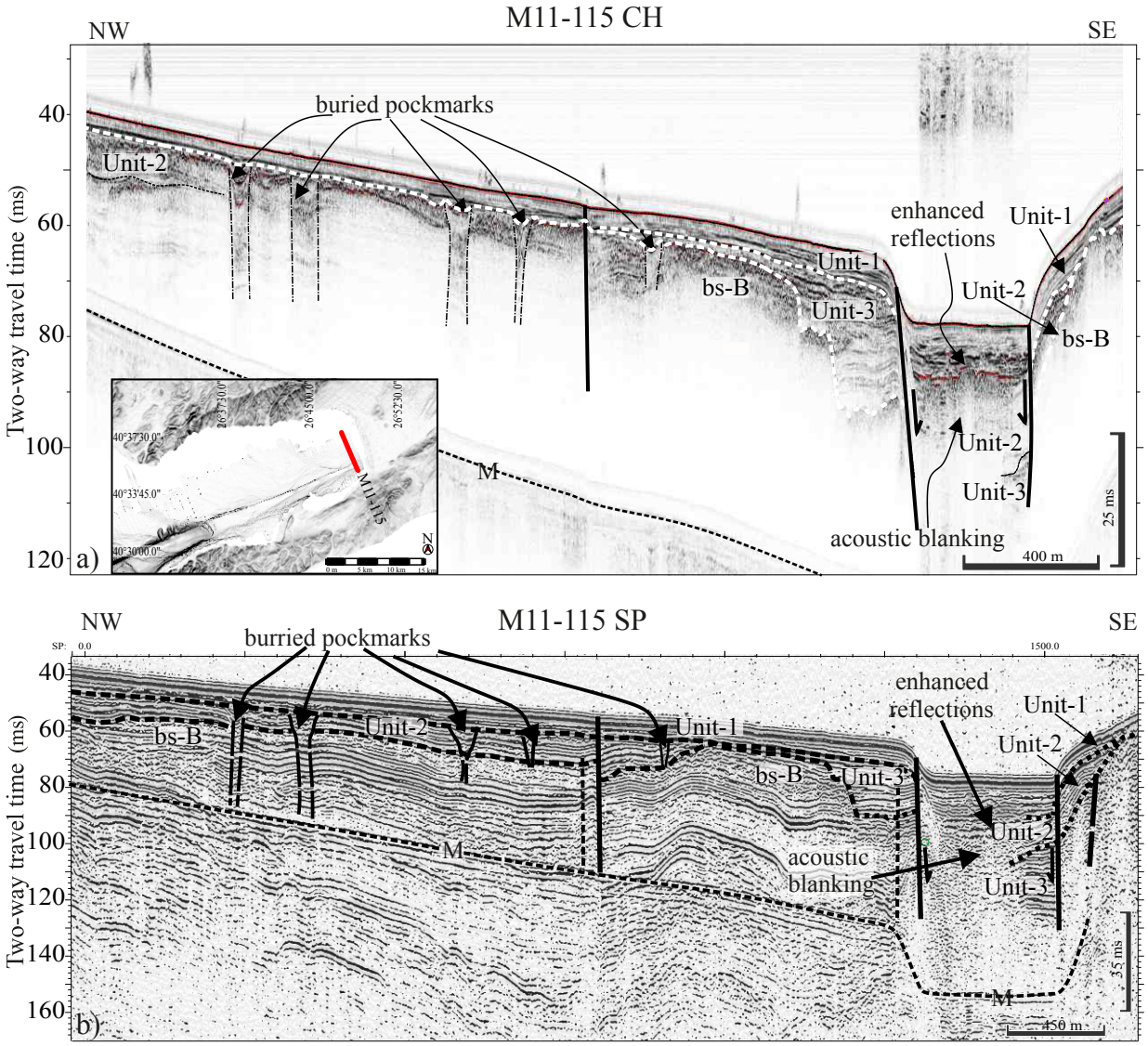

Figure 6. High resolution seismic (a) Chirp and (b) Sparker profiles M11-115 are showing gas-related structures in Unit-1 to Unit-3 units; bs-B basement, M multiple. Location in the inset.

subunit displays discontinuous low amplitudes and high-frequency reflections, which gain a chaotic configuration on the northern edge of the incised valley as shown by seismic profiles M11-71 SP and M11-91 SP (Figures 8, 9). The thickness of the lower subunit ranges from 0.5 m to 4.25 m, thickening towards south and westward. In the southeastern part of the seismic profile M11-89 SP, this facies includes in its upper part approximately 10 m thick lenticular berm deposits (Figure 5). Moreover, in seismic profiles M11-71SP- and M11-53 SP, a number of gas-related structures (mostly pockmarks) are observed (Figures 8 and 10).

The upper subunit is mainly characterized by continuous, subparallel, high-amplitude, and low-frequency reflectors. It probably represents the seabed on the shelf. Similar to the lower subunit, it thickens towards the basin and the incised valley. Its thickness is generally about 4.5 m, although it may reach up to 40 m (Figure 8b). This facies was sampled, analyzed, and dated on the northern shelf where it comprises mainly greenish-grey mud interbedded with sands and shells represented by bivalves, gastropods, ostracods, and echinoids. ^{14}C dating of these sediments indicates that they were deposited during the most recent sea-level high stand, forming a Holocene post-transgression unit (Çağatay et al., 1998).

3.3. Gas and fluids

Gas-related structures in the eastern shelf occur along both sides of the incised valley of the Ganos Fault (Figure 12) and

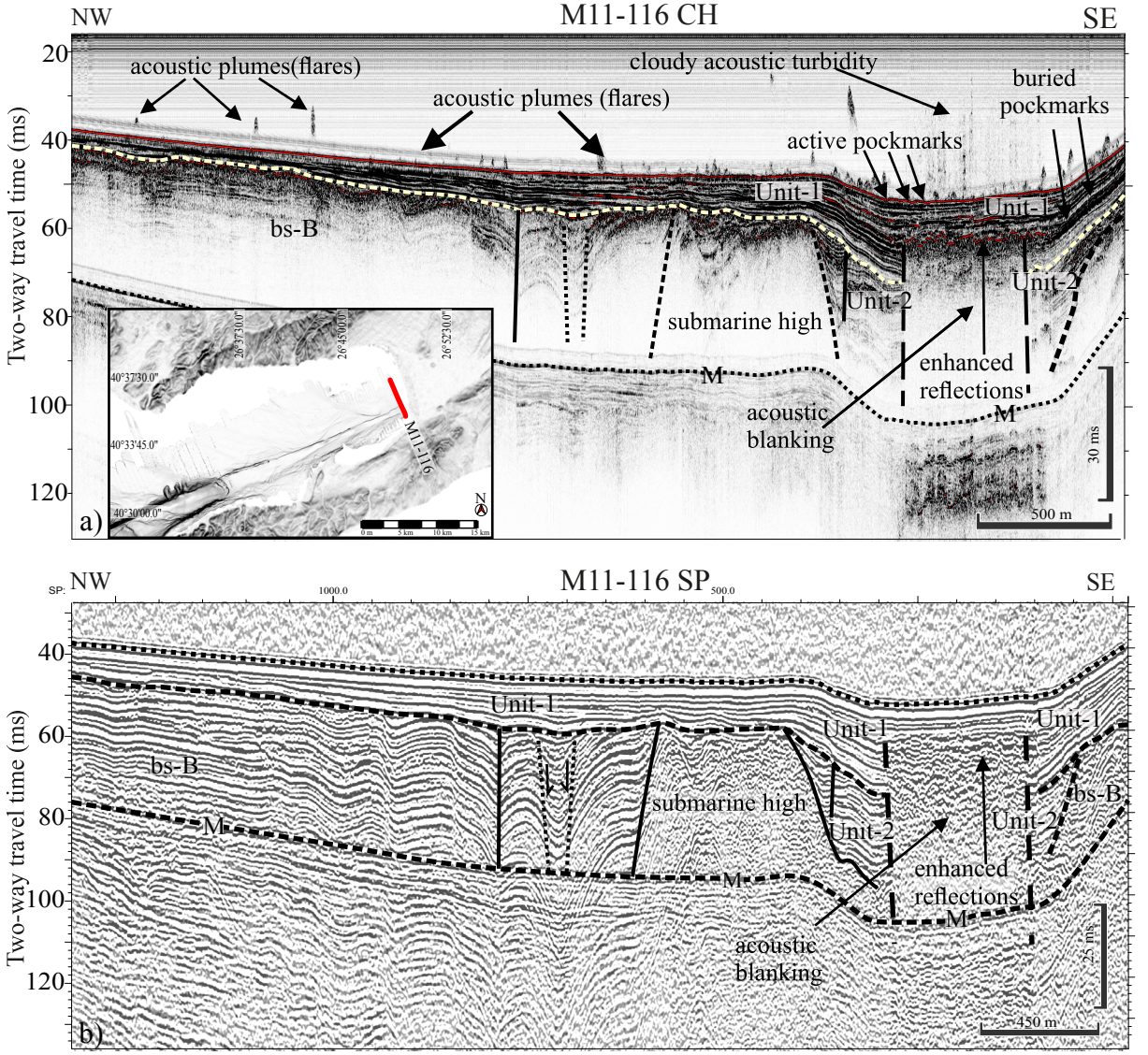

Figure 7. Interpretation of (a) Chirp-sonar and (b) Sparker profile M11-116. Profiles showing acoustic blanking with upper enhanced reflections within Unit-1 and Unit-2; bs-B basement, M multiple. Location in the inset.

may be described as under two groups: gas accumulation and gas escape features. Gas accumulation features form in subbottom sediments and includes enhanced reflections, acoustic blanking (or blanket), acoustic turbidity, acoustic curtain, and acoustic columns. Gas escape structures are driven by fluid expulsion from the seafloor and are primarily domes, pockmarks, and water-column features such as acoustic plumes and cloudy turbidity. Each feature will be described based on the most representative sparker (SP) and Chirp (CH) profiles.

3.3.1. Gas accumulation features

3.3.1.1. Enhanced reflectors

Enhanced reflectors are the most common features observed in the study area. They are characterized by enhanced amplitudes occurring both in shallow and deep levels of the units. They generally fade out rapidly with distance and are commonly associated with other gas structures, such as acoustic blanking and acoustic turbidity. In Chirp profiles, they mostly appear as a distinct and convex dark boundary on top of these structures, while in the sparker profiles, they are highlighted by high-amplitude, coherent to broken, and parallel to chaotic reflectors (Figures 6, 7, 10, and 20). The lateral continuity of the enhanced reflectors may reach up to > 2 km.

3.3.1.2. Acoustic blanking (or blankets)

Acoustic blanking is associated with transparent seismic facies with ghost internal reflections (Figures 14 and 15) that may be interpreted as gas-related structures

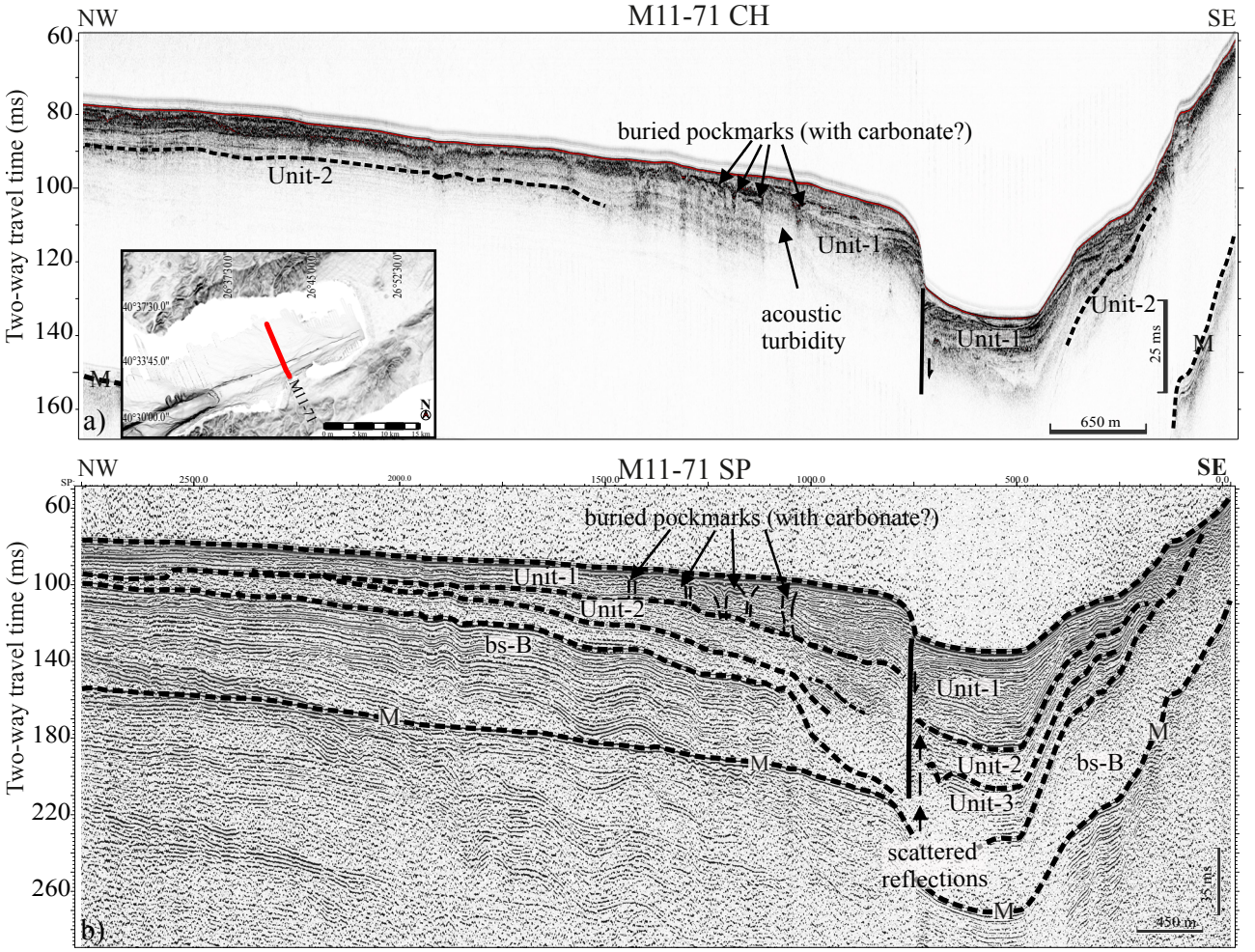

Figure 8. Interpretation of (a) Chirp and (b) Sparker profile M11-71. Buried pockmarks are seen in Unit-1. The main seismic sequences are Unit-1 to Unit-3. bs-B basement, M = multiple. Location in the inset.

developing more frequently close to the incised valley (Figure 12). In the Chirp profile of the M11-116 CH (Figure 7a), this structure developed within the infill of the incised valley, while in the corresponding sparker profile, ghost reflectors are seen as broken or chaotic reflections with increased amplitudes, mimicking enhanced reflectors (Figure 7b). The acoustic blanking in the M11-116 (Figure 7) has a 500 m wide rectangular shape with sharp edges corresponding to tectonic structures and shows a convex upper boundary. In the central part of the study area, acoustic blanking is localized in the basement below a sharp angular unconformity, and its lateral extension is controlled by two faults (Figure 14). In this area, the acoustic blanking is topped by an enhanced reflection and acoustic turbidity. In the eastern part of the study area, the acoustic blanking affects the basement as well as Unit-3 (Figure 15), and it is identified by an upper strong and broken enhanced reflection completely masking seismic reflections in the Chirp profile.

3.3.1.3. Acoustic turbidity

Acoustic turbidity features are similar to acoustic blanking in Chirp profiles and mask most reflectors even though seismic penetration is not completely hampered and coherent reflection patterns are still visible despite reduced amplitudes. The acoustic turbidity zone is predominant at the northern side, near the northeastern corner of the deep trough of the Saros Gulf. Its upper boundary lies at a depth of –79 m to –130 m below the present sea level (Figure 17). This type of gas-related structure is common in Unit-3, and Unit-2 around the incised valley. In the sparker profiles, acoustic turbidity displays a variable amount of disturbance with common chaotic reflections and are generally topped by enhanced reflections (Figures 8, 10, 13, 14 and 16).

3.3.1.4. Acoustic curtains

This gas feature is characterized by a transparent pattern in the Chirp profiles, with a characteristic convex-shaped upper boundary resembling a hyperbola (Figure 16). Below

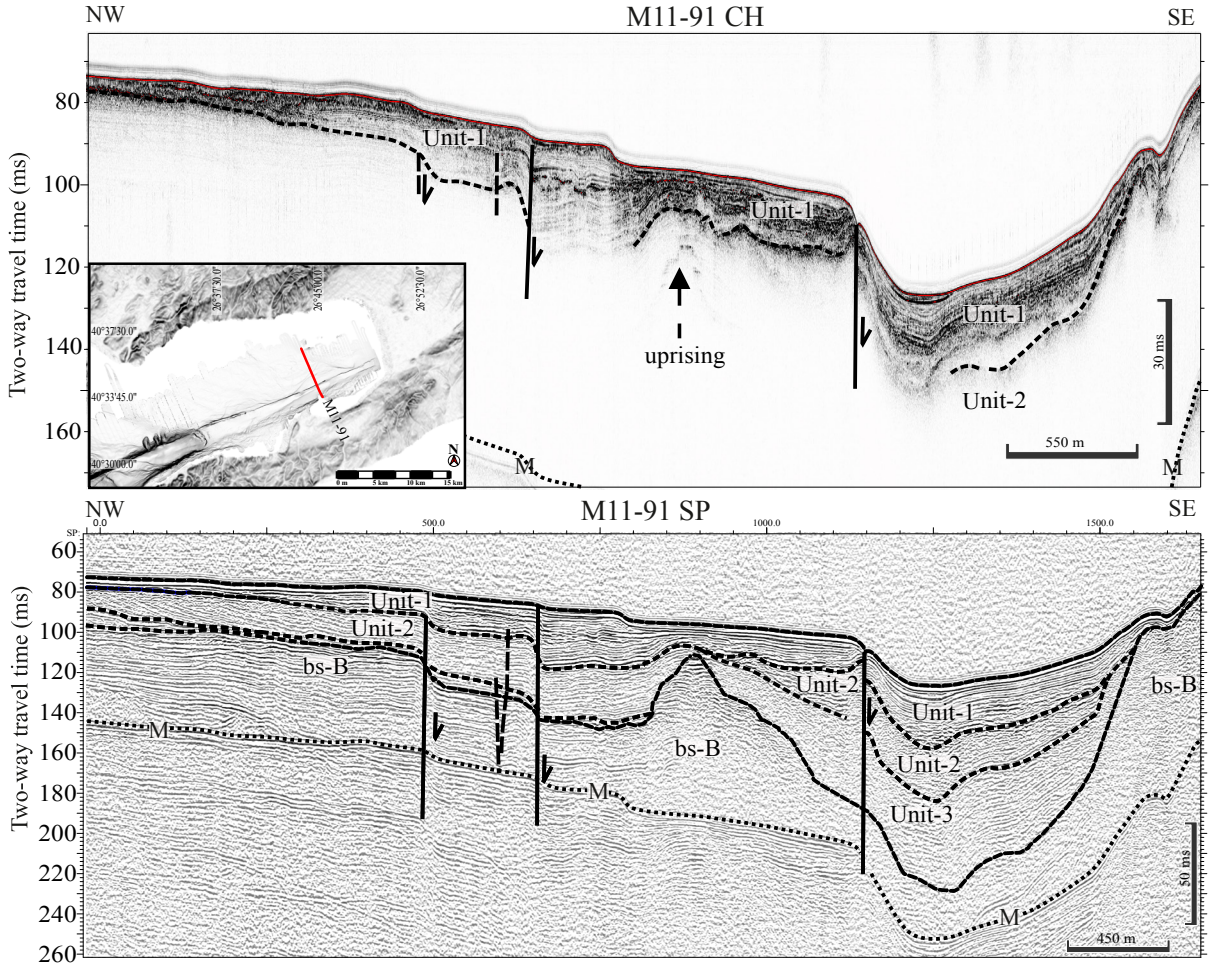

Figure 9. Interpretation of Chirp (top) and Sparker profile (bottom) M11-91. Seismic images are showing tectonic features and main seismic sequences as Unit-1 to Unit-3. bs-B basement, M=multiple. Location map in the inset.

this boundary, two well-marked, strong and continuous parallel reflectors are observed. These gently dipping reflectors are the continuation of the Unit-2 sedimentary layers (Figure 16).

3.3.1.5. Acoustic columns

The acoustic columns are vertical and narrow (20–90 m) columnar features with lengths between 7 m and 35 m, characterized by acoustic transparency in Chirp profiles and acoustic disturbances in sparker profiles (Figures 15 and 18). These structures mainly occur close to the incised valley where the acoustic blanking domains are observed. However, their association with other gas-related structures, such as pockmarks, domes, and acoustic plumes, is also common, extending downward within the underlying sediments (Figures 16 and 19).

3.3.2. Gas escape features

3.3.2.1. Domes

Small dome-shaped features frequently occur at the seafloor in the study area, sizing 10 m in height and less than 100 m in diameter. In Chirp profiles, the domes are seen as transparent structures, cutting the seabed and the underlying sub-bottom sediments with sharp edges and strong reflections at the top (Figures 18 and 19). In the Sparker profiles, they are distinguished by their characteristic narrow acoustic pipes, extending from the domes downward into the sub-bottom sediments. The acoustic pipes display vertically stacked, high amplitude reflectors, which appear folded in the upper parts, and with low amplitude discontinuous reflectors and chaotic facies below (Figures 18 and 19).

3.3.2.2. Pockmarks

Pockmarks are V-shaped depressions developing on the seafloor. They are common within the incised valley, and they can be associated with acoustic turbidity, showing a wide range of sizes, between tens and hundreds of meters in width and between 2 and 10 m in height. We observe two types of pockmarks, active and buried, the latter presently cropping out at the seafloor and venting fluids

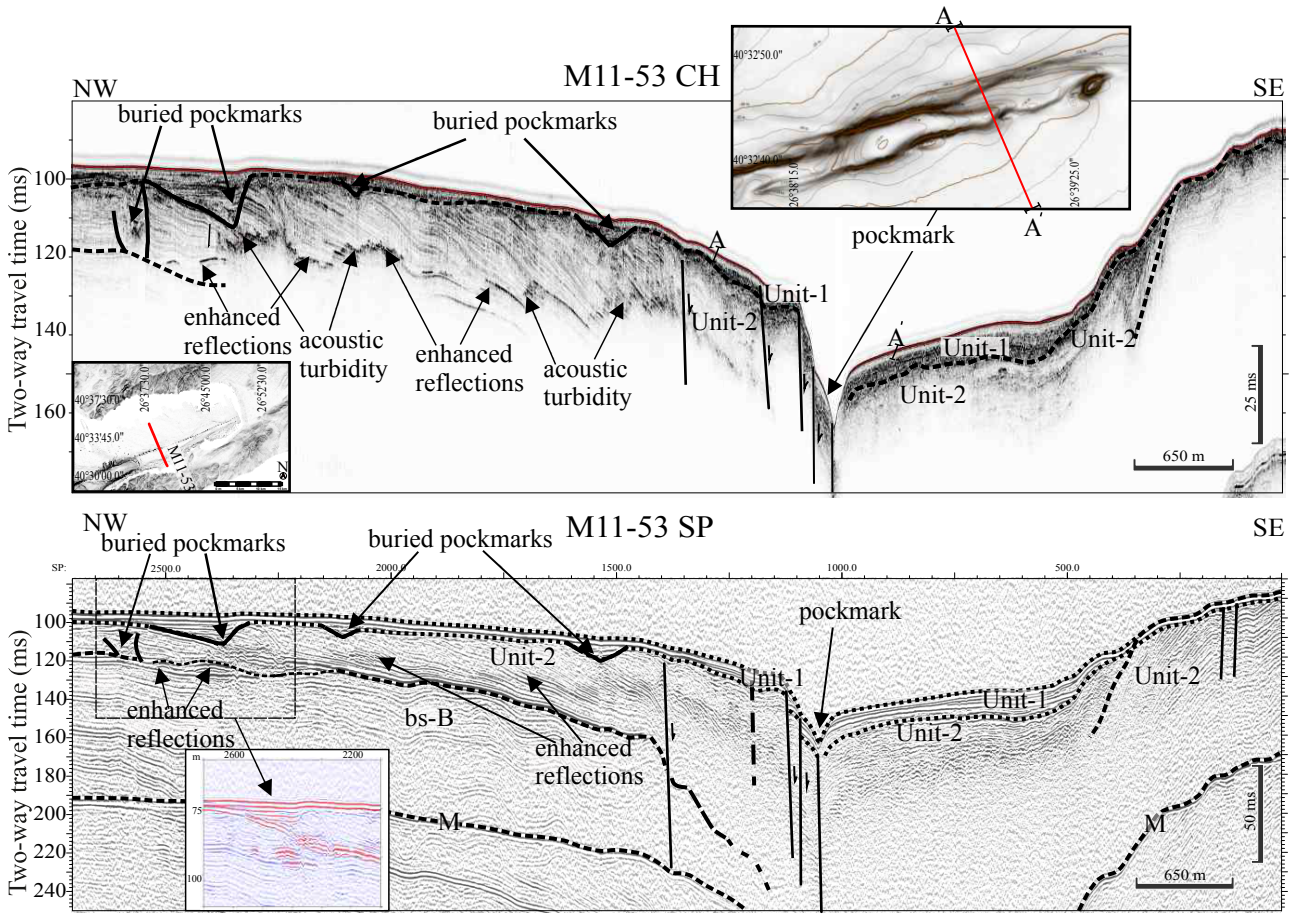

Figure 10. Interpretation of Chirp (top) and Sparker profile (bottom) M11-53 across the incised valley, showing buried and active pockmarks seems to form in the Unit-1 and Unit-2. Enhanced reflections are common in Unit-2. bs-B basement, M multiple. Location map in the inset.

(Figures 7). A giant active pockmark is observed on the M11-53 in the incised valley (Figure 10). Buried or ancient pockmarks are found at different depths in the upper part of Unit-2, particularly at the base of the Unit-1, about 4-5 m below the seafloor (Figure 7). In Chirp profiles, the buried pockmarks vertically extend 2 to 26 m downward into the subbottom sediments. Their downward extensions are generally transparent narrow columnar structures with dark-colored stains (Figures 6 and 10). In sparker profiles, the columns represent acoustically disturbed structures with high and low amplitude down-warped parallel and chaotic reflectors (Figure 6b).

3.3.2.3. Acoustic plumes (flares)

They appear as diffractions in the water column (Figures 7, 14, 16, 20) propagating from the seafloor above pockmarks and domes, rising about 10 m above the seafloor. When not directly associated with a seafloor feature, they could be confused with other targets, such as shoals of fish and it is crucial to verify the occurrence with repeated passages or crossing lines. In the incised valley, these features occur in groups and form plume fields. Here, they are usually associated with acoustic blanking and turbidity in the sediments (Figures 7 and 20).

3.3.2.4. Cloudy acoustic turbidity

This feature is observed in the water column above the incised valley, where plume fields develop; it appears most common in the upper layers above acoustic plumes. In Chirp profile M11-116 (Figure 7), acoustic turbidity appears as a "stained water sheet" without any characteristic internal texture.

4. Discussion and conclusion

The combined effect of the E-W dextral shear and accompanied N-S extension of the NAF in the Saros Gulf area resulted in a westward-widening and -deepening basin. Tectonic deformation was spread in a relatively wide deformation zone, which appears progressively focusing towards the basin center during the most recent tectonic phases. The transtensive triangular topographic depression is asymmetric, with broad northern and

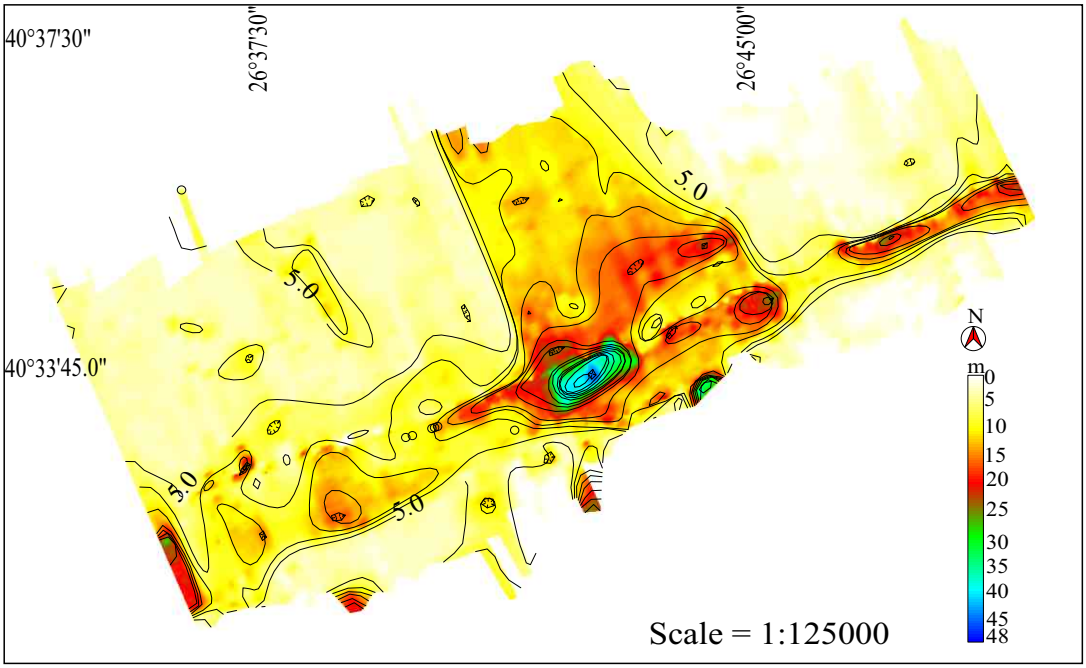

Figure 11. Isopach map displaying sediment thickness of Unit 1.

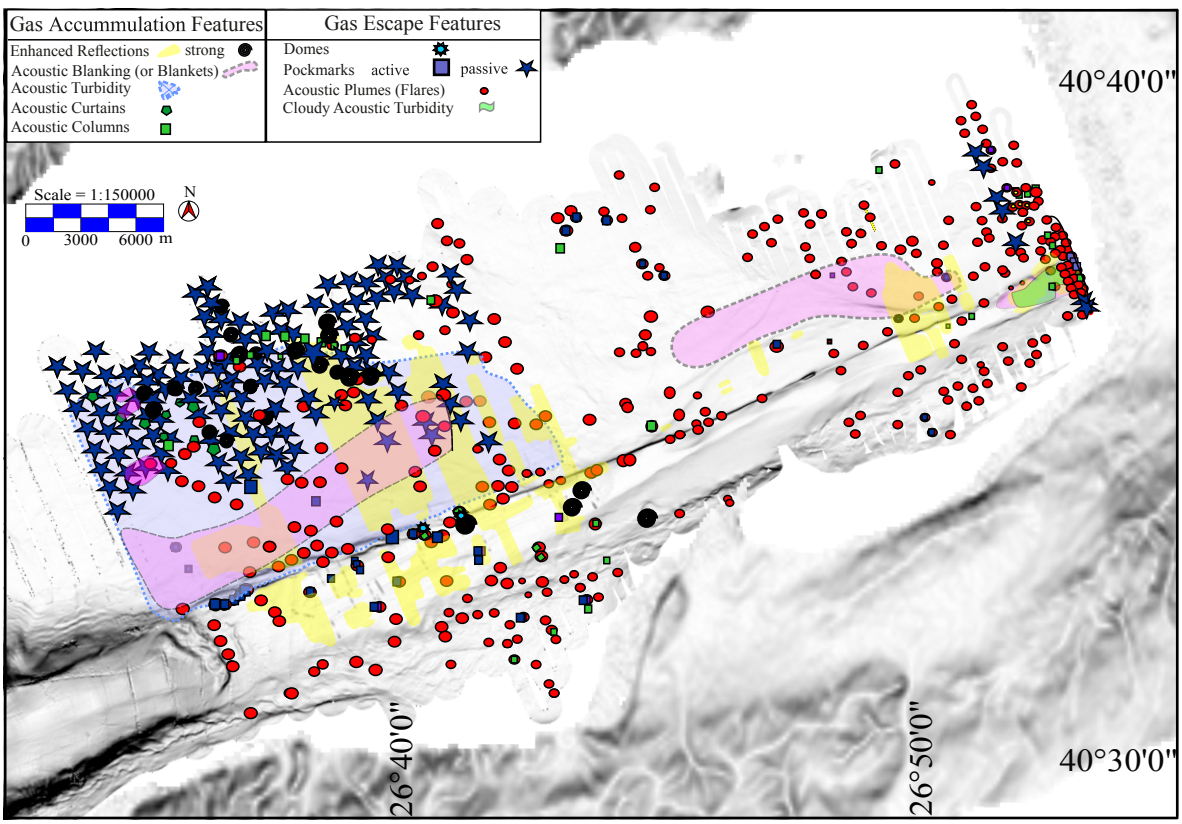

Figure 12. Distribution of gas accumulation and gas escape features. Bathymetry (slope map) from R/V Urania 2005 and 2011 cruises; topography from NOAA National Geophysical Data Center ETOPOI Global Relief (Amante and Eakins,2009).

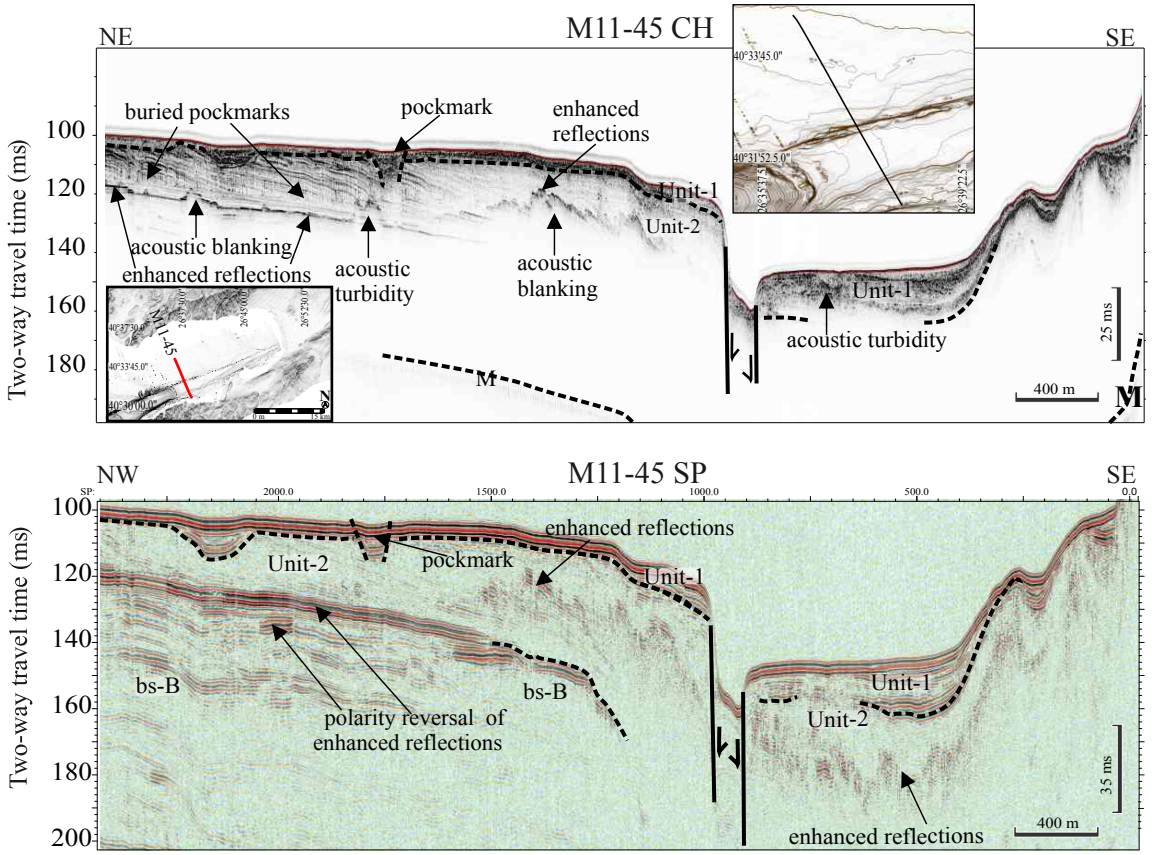

Figure 13. Interpretation of Chirp (top) and Sparker (bottom) profile M11-45, showing polarity reversal of enhanced reflections. Surficial and buried pockmarks are also seen in the northern side of the valley. Seismic section is also indicating that Unit-2 is pervasively affected by acoustic blanking and enhanced reflections. bs-B basement, M = multiple.

eastern shelves narrowing towards the south. Quaternary sediments accumulate in the basin as characteristic seismostratigraphic sequences, controlled by global glacio-eustatic sea-level fluctuations and tectonic deformation along the Ganos Fault. Sequence boundaries of the three depositional units recognized can be tentatively matched with the global sea-level curve. In this way, we could assume that they developed during Pleistocene to Holocene glacial-interglacial cycles. Unit-1 and Unit-3 accumulated during the interglacial periods and formed transgressional/highstand sequences, whereas Unit-2 deposited during a lowstand phase. The transgressional units are characterized by upward-fining successions and, thus, created seals at their tops to form favorable niches for gas accumulation. Thus, most gas accumulation structures probably occurred during transgressive/highstand phases. The progradational Unit-3 appears heavily eroded at its top, therefore, perhaps unfavorable for gas accumulation.

Although direct gas analyses are not available, possible sources can be considered as mixtures of microbial methane, thermogenic methane, and other hydrocarbons, such as ethane, butane, and propane such as proposed for the Marmara Sea (Bourry et.al, 2009; Dupré et al., 2015). Microbial methane is formed from the decomposition of organic debris by bacteria in an anoxic environment (Floodgate and Judd, 1992). The eastern shelf, which was rapidly accumulating the fine-grained and organic-rich muddy sediments of the Meriç River and the Kavak Creek, might have provided a suitable environment (Floodgate and Judd, 1992). The thermogenic methane is created from the decomposition of organic debris by geological processes under deep earth conditions. It might have been delivered to the surface in the eastern shelf by the dense net of fractures and faults highlighted by the morphostructural map (Figure 3) as described for the deep Marmara basin (Bourry et. al, 2009; Dupré et al., 2015). The Thrace Basin Eocene rocks, constituting the stratigraphic basement, represent one of the major hydrocarbon-bearing basins in the region. If the presence of thermogenic gas seeps will be confirmed, the Ganos Fault could have probably played an important role in providing a direct connection of the oil reservoirs to the surface, causing upward migration. The gas accumulation in the eastern shelf just north of the incised valley is much larger compared to its southern

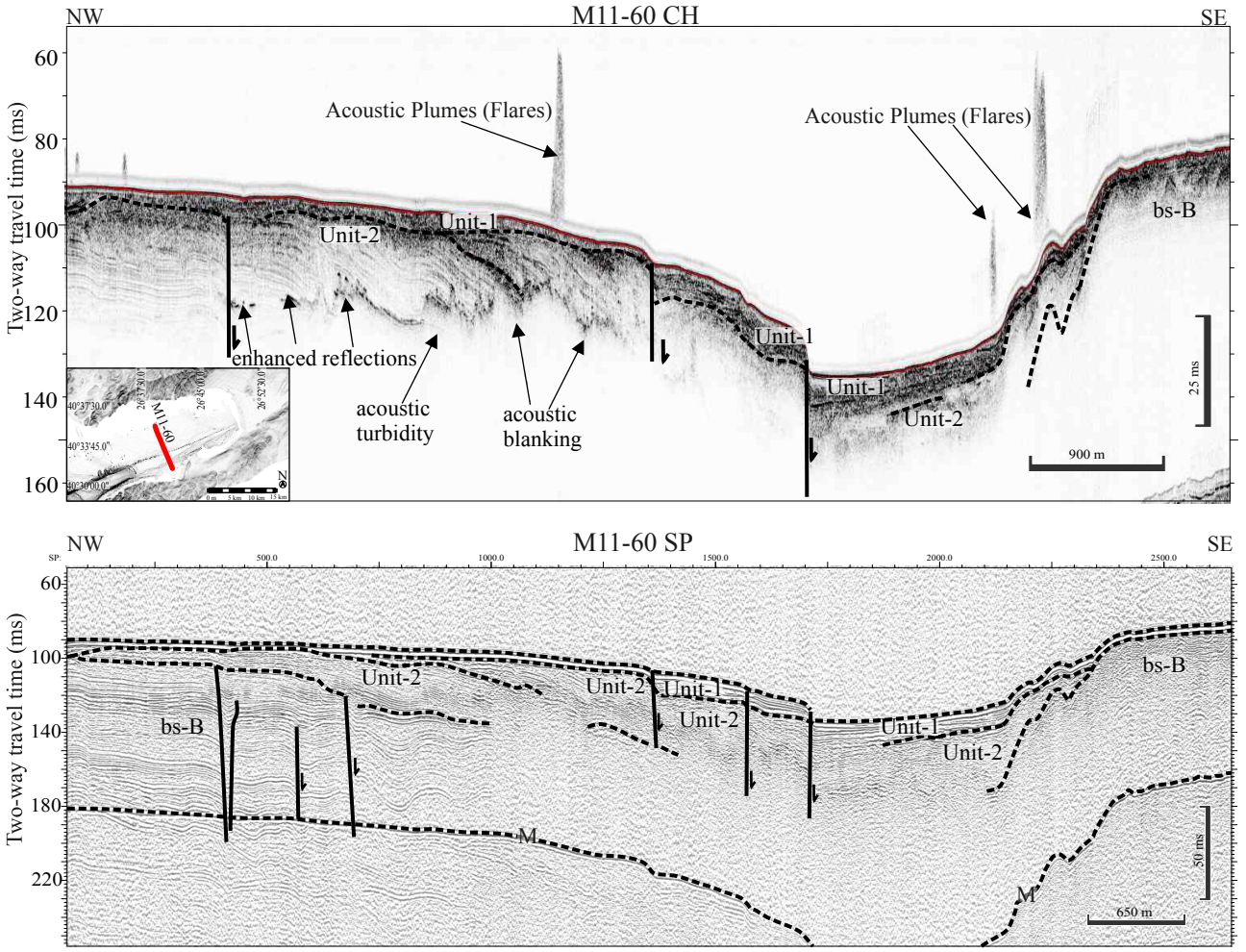

Figure 14. Interpretation of Chirp (top) and Sparker (bottom) profile M11-60 collected across central part of the incised valley. Acoustic blanking masks reflections from the basement in both Chirp and Sparker profiles. Acoustic plumes in the water column show gas escape is being in the incised valley. M = multiple. Location in the inset.

correlative and covers an area of about 120 km^2 (Figure 12). Here, gas and fluids are mostly observed as acoustic blanking, acoustic turbidity, and acoustic columns in a depth range between 7 and 10 m below the seafloor. Acoustic blanking occurs both in the northern side and the incised valley, close to the northeastern coast of the Gulf (Figure 12). This gas structure probably develops in depositional units, having high porosity contrast between the seal and reservoir facies. Acoustic turbidity is observed in the northern side, near the northeastern corner of the deep trough of the Saros Gulf. This gas structure usually forms where impervious clay-rich sediments exist (Fannin, 1980). Acoustic columns are commonly observed in the northern side in association with buried pockmarks. They should indicate upward migration of gas or fluids in the sediments.

The gas escape features in the incised valley and the neighboring areas are characterized mainly by domes, pockmarks, acoustic plumes, and cloudy acoustic turbidity. This is the case of three aligned circular dome-shaped structures occurring south of the acoustic turbidity area visible in the multibeam bathymetry, Chirp and Sparker profiles. These features may represent the initial stage of pockmark formation and probably originate from the displacement of pore waters within Unit-1 and -2 during gas and fluid escapes (Figure 18 and 19). Remarkably, one of them resembles the shape of a mud volcano characterized by down bending layers at its flanks (Figure 18). Pockmarks originate where fluids or gas escape from the seabed, causing reworking of sediments and creating v-shaped depressions. These structures are common in the southwestern part of the northern shelf. Two types of them are observed: active and buried (inactive) pockmarks. Active pockmarks are located mostly in the incised valley, close to the deep trough of the Saros Gulf. The buried pockmarks are abundant in the northern side

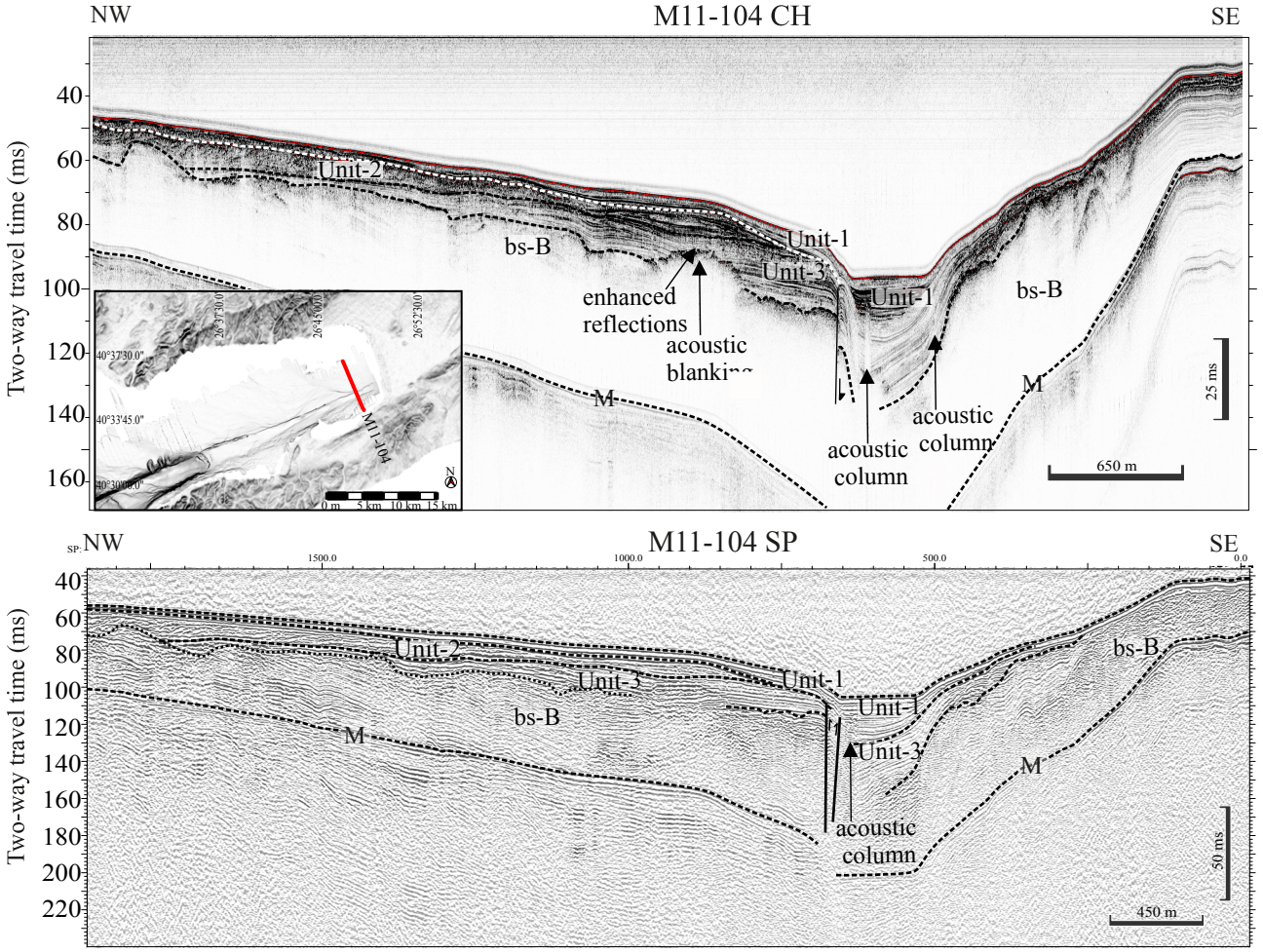

Figure 15. Interpretation of Chirp (top) and Sparker (bottom) profile M11-104. Gas accumulation features are located in Quaternary and Palaeogene sediments. bs-B basement, M = multiple. Location in the inset.

where acoustic turbidity was observed (Figure 12). They occur on top of Unit-2 and are sealed by the sediments of Unit-1, indicating that they were active before 12 ka. Acoustic plumes predominate over all the other gas-related structures and are seen in the incised valley and the adjacent shelf areas (Figure 12). These structures show incipient seepage from the seafloor, ascending along the water column. The cloudy acoustic turbidity in the water column is perhaps formed by sediment resuspension at gas seepages. Acoustic plumes and cloudy acoustic turbidity seem to be associated in the northern side with gas accumulation in the sediments.

Figure 12 reveals that on the eastern shelf, gas emissions mainly occur through pockmarks and acoustic plumes. The spatial distributions of these structures indicate that gas venting is driven by tectonic activity since gas/fluid flows by fault distribution. The occurrence of the numerous inactive pockmarks on the northern fault block on top of Unit-2 may be considered as evidence for vigorous gas emission before the Holocene transgression during the last sea-level low stand. Unit-2 formed during the Würm glacial stage and the following early phase of deglaciation when the sea level dropped as much as 120 m below the present-day sea level (van Andel and Lianos, 1984; Aksu et al., 1987; Çağatay et al., 1998). We could assume that during its deposition, Unit-2 trapped abundant gas and fluids of both thermogenic and biogenic origin, which remained stored in the sediments until the Holocene transgression. In fact, we can speculate that the balance between pore and overburden pressures probably broke during the Holocene transgression, inhibiting the leakage of the pore fluid, as suggested by pockmarks on top of Unit-2. The vicinity of the active pockmarks to the structurally controlled incised valley may indicate that the Ganos Fault is highly effective in breaking the pressure's balance during major earthquakes, also during sea-level highstands.

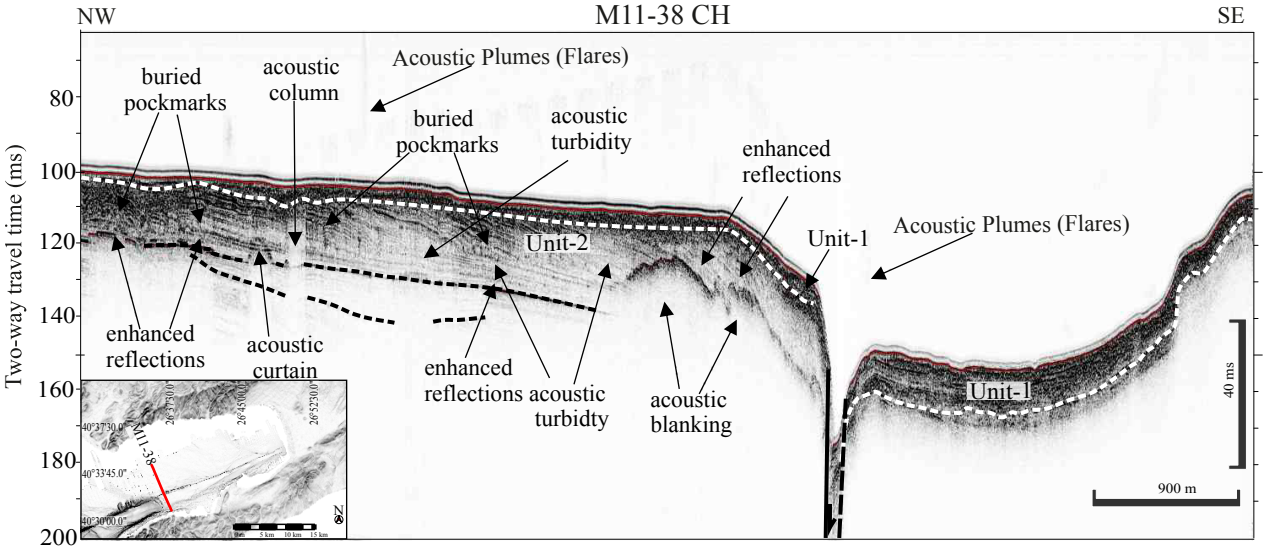

Figure 16. Interpretation of Chirp profile M11-38 showing seismic gas accumulation and gas escape features. bs-B basement, M = multiple. Location in the inset.

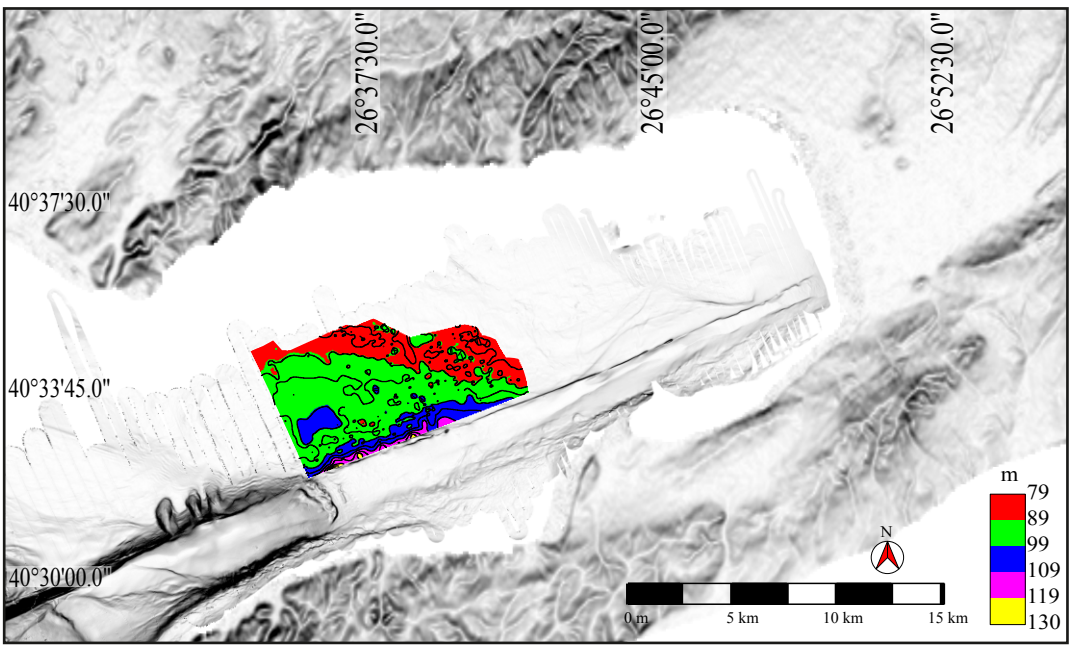

Figure 17. Colour-contour map displaying the upper boundary of the acoustic turbidity zone.

The acoustic plumes of Unit-1 developed not only above buried pockmarks but almost everywhere along both sides of the incised valley (Figure 12). Unit-1 formed along with the Holocene transgression and therefore developed an upward-fining transgressive sequence with a muddy impermeable cap during the highstand. Under normal conditions, gas cannot be expelled from such a lithology unless these sediments experience deformation, resulting from faulting or pore-pressure increase. The spatial and temporal analyses of the acoustic plumes suggest that the damage zone of the Ganos fault was effective in controlling degassing processes during earthquake-triggered ground shaking.

We can conclude that the Saros Gulf shelf represents an interesting target for combined seismological/geochemical monitoring experiments similar to those attempted in

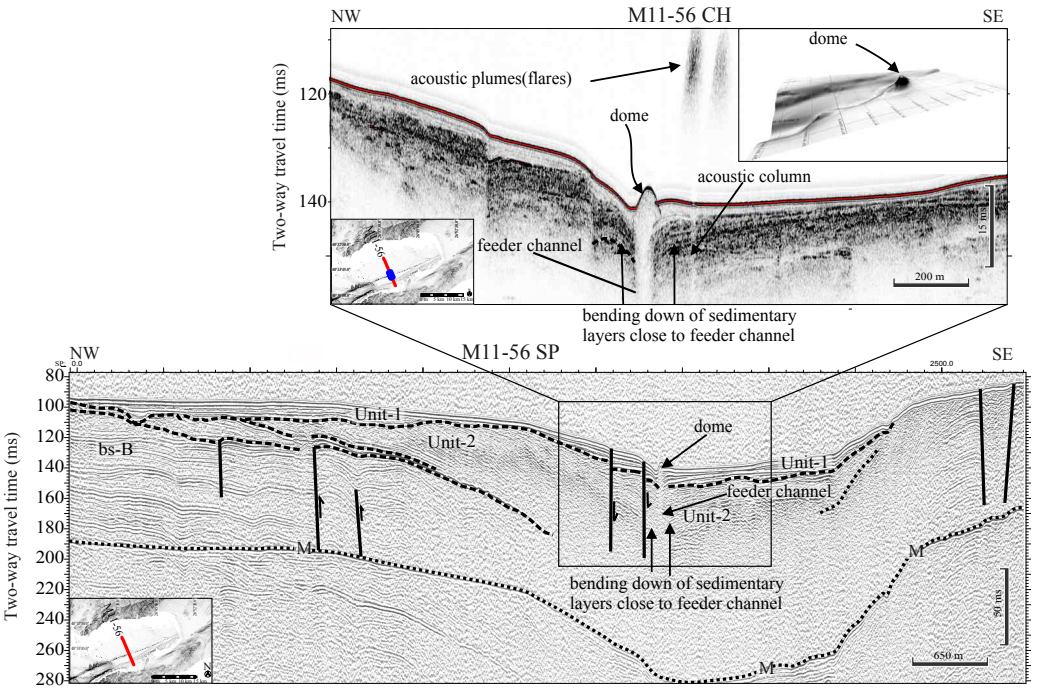

Figure 18. Interpretation of Chirp (top) and Sparker (bottom) profile M11-56. Note the downward bending of sedimentary layers toward the feeder channel indicating collapse. The feeder zone exhibits a transparent texture without any reflection. This structure resembling a mud volcano is accompanied by gas escape features. Location in the inset.

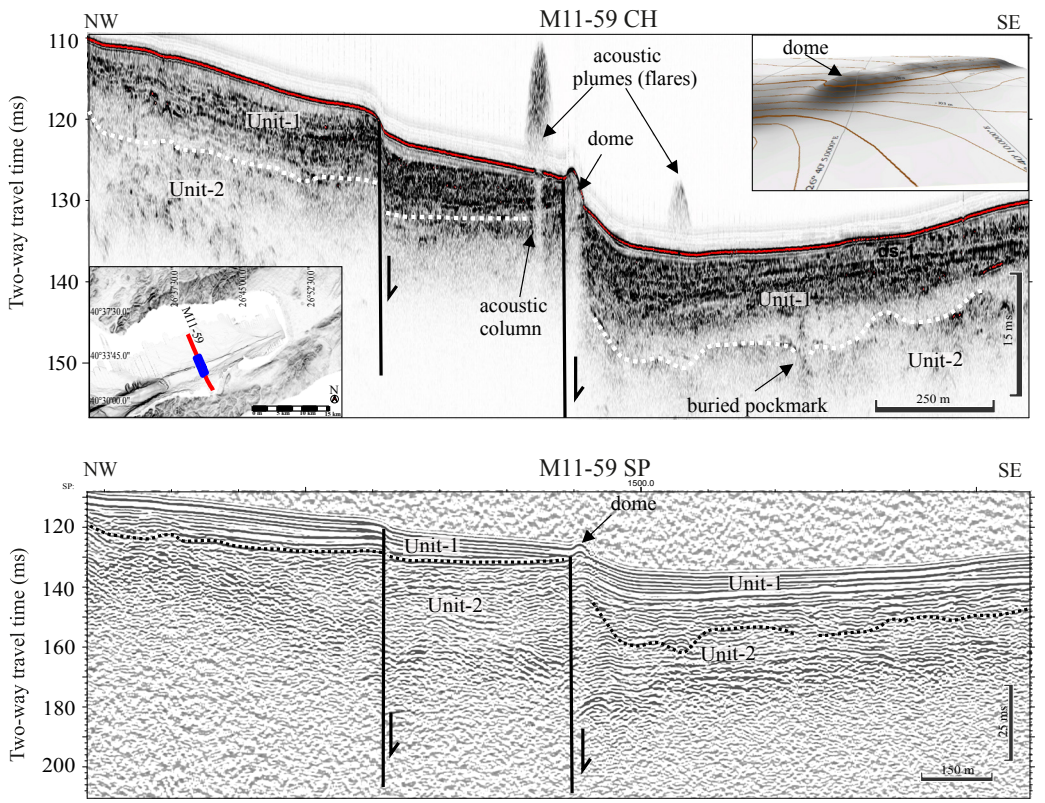

Figure 19. Chirp-sonar (top) and Sparker (bottom) seismic reflection M11-59 profile, showing that gas escape features, such as dome and acoustic plumes in the water column are mostly associated with tectonic movements. bs-B basement. Location in the inset.

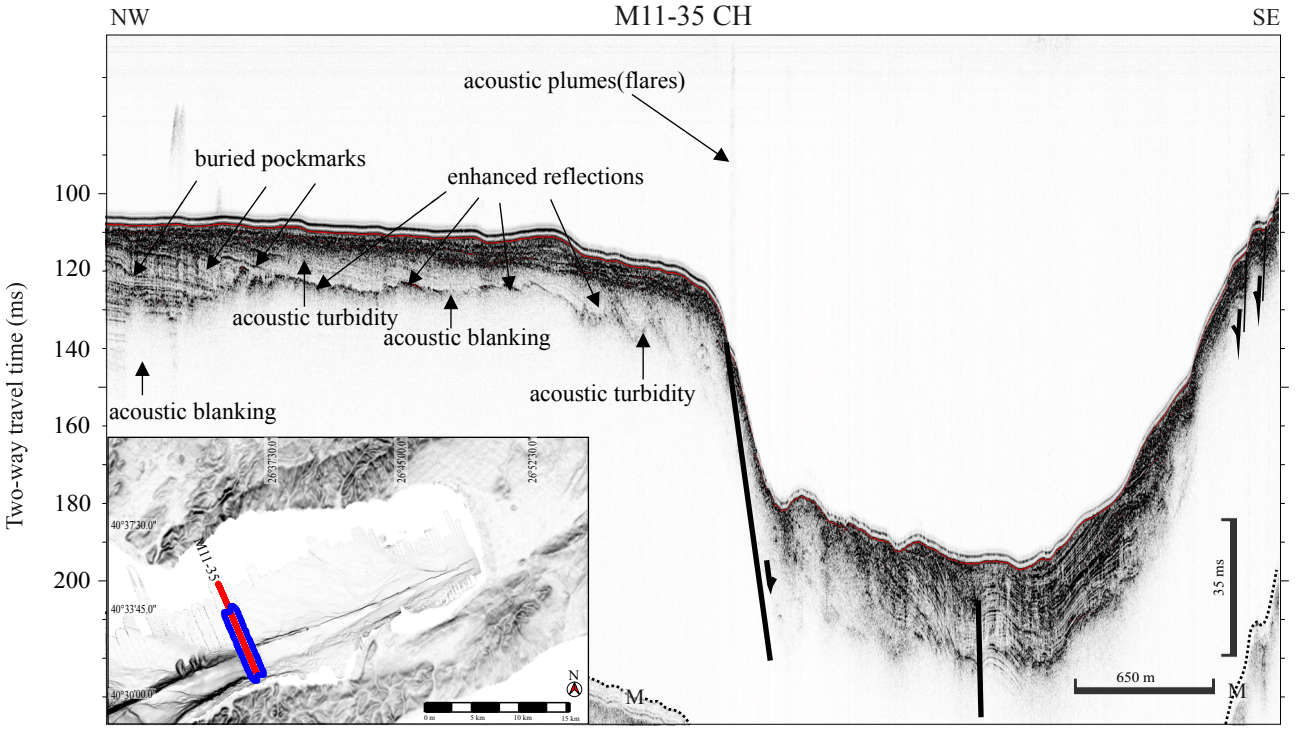

Figure 20. Chirp-sonar profile M11-35 showing gas seeps in the water column associated with acoustic blanking and turbidity.

the Gulf of İzmit after the 1999 Mw = 7.6 earthquake (Gasperini et al., 2012; Embriaco et al., 2013). In fact, it includes several peculiar characters such as a very focused active deformation zone, a vigorously degassing seafloor, the diffuse presence of tectonic-controlled gas and fluid reservoirs in the sediments and intense seismicity, culminating both with moderate magnitude events (1975, 1983, 2014) and large historical earthquakes (1912) (Figure 1a). Under such conditions, an experiment involving the use of a long-term seafloor observatory could shed some light on the complex relationship between seismicity and fluid flow in the subsurface, opening the door to earthquake precursors studies.

Acknowledgments

We thank all of the scientific staff and the crew members of R/V Urania, especially Captain Gentile and Captain Lubrano. Şebnem Önder acknowledges the post-doc research grant [1059B191500404] by TUBITAK BIDEB 2219. Önder is grateful for the support of Marco Ligi and Giovanni Bortoluzzi. HIS Markit is acknowledged for the university user license grant.

References

Aksoy ME, Meghraoui M, Vallée M, Çakır Z (2010). Rupture characteristics of the A.D. 1912 Mürefte (Ganos) earthquake segment of the North Anatolian fault (western Turkey). Geology 38: 991–994. doi: 10.1130/G31447.1.

Aksoy ME (2021). The 9 August 1912 Mürefte-Şarköy earthquake of the North Anatolian Fault. Mediterranean Geoscience Reviews 3: 95-114.

Aksu AE, Piper DJW, Konuk T (1987b). Quaternary growth patterns of the Büyük Menderes and Küçük Mederes Deltas, Western Turkey. Marine Geology 76: 89-104.

Alpar B, Yaltırak C (2002). Characteristic features of the North Anatolian Fault in the eastern Marmara region and its tectonic evolution. Marine Geology 190 (1–2): 329-350.

Amante C, Eakins BW (2009). ETOPO1 1 Arc-Minute Global Relief Model: Procedures, Data Sources and Analysis. NOAA Tech. Memo. NESDIS NGDC-24 19. Colorado, USA: NOAA. doi: 10.1594/ PANGAEA. 769615

Berckhemer H (1977). Some aspects of the evolution of marginal seas deduced from observations in the Aegean region. In: Biju-Duval B, Montadert L (editors). International Symposium on the Structural History of the Mediterranean Basins. Split, Yugoslavia. pp. 303-314.

Bourry C, Chazallon B, Charlou JL, Donval JP, Ruffine L et al. (2009). Free gas and gas hydrates from the Sea of Marmara, Turkey: Chemical and structural characterization. Chemical Geology 264 (1-4): 197-206. doi: 10.1016/j.chemgeo.2009.03.007

Çağatay MN, Görür N, Alpar B, Saatçılar R, Akkök R et al. (1998). Geological evolution of the Gulf of Saros, NE Aegean Sea. Geo-Marine Letters 1: 1–9. doi: 10.1007/s003670050045

Davatzes NC, Aydın A (2003). Overprinting faulting mechanisms in high porosity sandstones of SE Utah. Journal of Structural Geology 25: 1795–1813. doi: 10.1016/S0191-8141(03)00043-9

Dewey JF, Şengör AMC (1979). Aegean and surrounding regions: Complex multiplate and continuum tectonics in a convergent zone. GSA Bulletin 90 (1): 84–92. doi: 10.1130/0016-7606(1979)90<84:AASRCM>2.0.CO;2

Dupré S, Scalabrin C, Grall C, Augustin JM, Henry P et al. (2015). Tectonic and sedimentary controls on widespread gas emissions in the Sea of Marmara: Results from systematic, shipborne multibeam echo sounder water column imaging. Journal of Geophysical Research: Solid Earth 120: 2891– 2912. doi: 10.1002/2014JB011617

Embriaco D, Marinaro G, Frugoni F, Monna S, Etiope G et al. (2013). Monitoring of gas and seismic energy release by multiparametric benthic observatory along the North Anatolian Fault in the Sea of Marmara (NW Turkey). Geophysical Journal International 196 (2): 850-866.

Emre Ö, Duman TY, Özalp S, Elmacı H, Olgun S, Şaroğlu F (2013). Active fault map of Turkey with an explanatory text 1:1,250,000 scale. Special Publication Series 30. Ankara, Turkey: General Directorate of Mineral Research and Exploration.

Eriş KK (2007). Middle Pleistocene to recent sea level changes in the Sea of Marmara. PhD, İstanbul Technical University, İstanbul, Turkey (in Turkish with English abstract).

Erol O, Çetin O (1995). Marmara Denizi'nin Geç Miyosen-Holosen'deki evrimi. In: Meriç E (editor). İzmit Körfezi Kuvaterner İstifi. Deniz Harp Okulu Komutanlığı Basımevi, İstanbul, Turkey. pp. 314-341.

Fannin NGT (1980). The use of regional geological surveys in the North Sea and adjacent areas in the recognition of offshore hazards. In: Ardus DA (editor). Offshore Site Investigation. London, United Kingdom: Graham and Trotman, pp. 5–22.

Floodgate GD, Judd AG (1992). The origins of shallow gas. Continental Shelf Research 12 (10): 1145–1156. doi: 10.1016/0278-4343(92)90075-U

Gasperini L, Stanghellini G (2009). SeisPrho: An interactive computer program for processing and interpretation of high-resolution seismic reflection profiles. Computers & Geosciences 35: 1497–1507. doi: 10.1016/j.cageo.2008.04.014

Gasperini L, Polonia A, Çağatay N, Bortoluzzi G, Ferrante V (2011). Geological slip rates along the North Anatolian Fault in the Marmara region. Tectonics 30:1-14 TC6001. doi:10.1029/2011TC002906, 2011

Gasperini L, Polonia, A, Del Bianco F, Etiope, G, Marinaro G et al. (2012). Gas seepage and seismogenic structures along the North Anatolian Fault in the eastern Sea of Marmara. Geochemistry, Geophysics, Geosystems 13 (10): 1-19.

Gasperini L, Aksoy E, Polonia A, Meghraoui M, Bianco F Del (2013). Geology and seismotectonics of the Gulf of Saros (NE Aegean Sea) along the seismotectonics of the Gulf of Saros (NE Aegean Sea) along the North-Anatolian Fault system. In: EGU General Assembly; Vienna, Austria. p.10180.

Gasperini L, Polonia A, Çağatay MN (2018). Fluid flow, deformation rates and the submarine record of major earthquakes in the Sea of Marmara, along the North-Anatolian Fault system. Deep Sea Research Part II: Topical Studies in Oceanography 153: 4–16. doi: 10.1016/j.dsr2.2018.03.004

Geli L, Henry P, Zitter T, Dupré S, Tryon M et al. (2008). Gas emissions and active tectonics within the submerged section of the North Anatolian Fault zone in the Sea of Marmara. Earth and Planetary Science Letters 274: 34-39.

Görür N, Okay AI (1996). A fore-arc origin for the Thrace Basin, NW Turkey. Geologische Rundschau 85: 662–668. doi: 10.1007/BF02440103

Görür N, Elbek Ş (2013). Tectonic events responsible for shaping the Sea of Marmara and its surrounding region. Geodinamica Acta 26:1–11. doi: 10.1080/09853111.2013. 859346

Görür N, Çagatay MN (2010). Geohazards rooted from the northern margin of the Sea of Marmara since the late Pleistocene: A review of recent results. Natural Hazards 54: 583–603. doi: 10.1007/s11069-009-9469-x

Hatem AE, Cooke M, Toeneboehn K (2017). Strain localization and evolving kinematic efficiency of initiating strike-slip faults within wet kaolin experiments. Journal of Structural Geology 101: 96–108. doi: 10.1016/j.jsg.2017.06.011

Jarvis A, Reuter HI, Nelson A, Guevara E (2008). Hole-filled SRTM for the globe version 3, from the CGIAR-CSI SRTM 90m database. CGIAR-CSI Consortium for Spatial Information.

Konca AÖ, Çetin S, Karabulut H, Reilinger R, Doğan U (2018). The 2014, Mw6.9 North Aegean earthquake: seismic and geodetic evidence for coseismic slip on persistent asperities. Geophysical Journal International 213: 1113-1120.

Kurt H, Demirbag E, Kuşçu I (2000). Active submarine tectonism and formation of the Gulf of Saros, Northeast Aegean Sea, inferred from multi-channel seismic reflection data. Marine Geology 165: 13–26. doi: 10.1016/S0025-3227(00)00005-0

Le Pichon X, Angelier J (1979). The Hellenic arc and trench system: A key to the neotectonic evolution of the eastern mediterranean area. Tectonophysics 60 (1-2): 1-42. doi: 10.1016/0040-1951(79)90131-8

Le Pichon X, Angelier J (1981). The Aegean Sea. Philosophical Transactions of the Royal Society of London. Series A. Mathematical and Physical Sciences 300 (1454): 357-372.

Myers R, Aydın A (2004). The evolution of faults formed by shearing across joint zones in sandstone. Journal of Structural Geology 26: 947– 966.

Polonia A, Gasperini L, Amorosi A, Bonatti E, Cağatay N et al. (2004). Holocene Slip rate of the North Anatolian Fault beneath the Sea of Marmara. Earth and Planetary Science Letters 427: 411-426.

Saner S (1985). Saros Körfezi dolayının çökelme istifleri ve tektonik yerleşimi, Kuzeydoğu Ege Denizi, Türkiye. Türkiye Jeoloji Kurumu Bülteni: 1–10 (in Turkish).

Sarı E, Çağatay M (2001). Distributions of heavy metals in the surface sediments of the Gulf of Saros, NE Aegean Sea. Environment International 26 (3): 169–173. doi: 10.1016/ S0160-4120(00)00097-0

Seyitoğlu G, Scott BC (1991). Age of the Alaşehir graben (West Turkey) and its tectonic implications. Geological Journal 31: 1-11.

Shackleton NJ, Opdyke ND (1973). Oxygen isotope and paleomagnetic stratigraphy of equatorial Pacific Core V28-238: oxygen isotope temperatures and ice volume on a 105 year and 106 year scale. Quaternary Research 3: 39-55. doi: 10.1016/0033-5894(73)90052-5

Siyako M, Burkan KA, Okay A (1989). Tertiary geology and hydrocarbon potential of the Biga and Gelibolu Peninsulas (in Turkish with English abstract). TAPG Bulletin 1 (3): 183–200.

Sümengen M, Terlemez İ, Şentürk K, Karaköse C, Erkan E et al. (1987). Gelibolu Yarımadası ve Güneybatı Trakya Tersiyer Havzası' nın stratigrafisi, sedimantolojisi ve tektoniği (in Turkish). The Mineral Research and Exploration 8128. Ankara, Turkey: General Directorate of Mineral Explaration and Research of Turkey.

Şengör AMC (1982). Ege'nin neotektonik evrimini yöneten etkenler (in Turkish). In: Erol O, Oygür V (editors). Batı Anadolu'nun genç tektoniği ve volkanizması. Ankara, Turkey: Congress of the Geological Society of Turkey Publications, pp. 59-72.

Şengör AMC, Görür N, Şaroğlu F (1985). Strike-slip faulting and related basin formation in zones of tectonic escape: Turkey as a case ctudy. In: Biddle KT, Christie-Blick N (editors). Strike-Slip Deformation, Basin Formation, and Sedimentation. 10. New York, USA: Society of Economic Paleontologists and Mineralogists Special Publication, pp. 227–264.

Şengör AMC, Tüysüz O, İmren C, Sakınç M, Eyidoğan H et al. (2005). The North Anatolian Fault: A new look. Annual Review of Earth and Planetary Sciences 33 (1): 37-112.

Şengor AMC, Zabcı C, Natalin B (2019). Continental Transform Faults: Congruence and Incongruence with normal plate kinematics. In: Duarte João C (editor). Transform Plate Boundaries and Fracture Zones. Amsterdam, Netherlands: Elsevier, pp. 169-247.

Tchalenco JS (1970). Similarities between shear zones of different magnitudes. Geological Society of America Bulletin 81: 1625–1640.

Taymaz T, Jackson J, Mckenzie D (1991). Active tectonics of the north and central Aegean Sea. Geophysical Journal International 106 (2): 433-490.

Tüysüz O, Barka A, Yiğitbaş E (1998). Geology of the Saros graben and its implications for the evolution of the North Anatolian Fault in the Ganos – Saros region, northwestern Turkey. Tectonophysics 293: 105–126.

Ustaömer T, Gökaşan E, Tur H, Görüm T, Batuk FG et al. (2008). Faulting, mass-wasting and deposition in an active dextral shear zone, the Gulf of Saros and the NE Aegean Sea, NW Turkey. Geo-Marine Letter 28: 171–193. doi: 10.1007/s00367-007-0099-6

van Andel TH, Lianos N (1984). High-resolution seismic reflection profiles for the reconstruction of postglacial transgressive shorelines: An example from Greece. Quaternary Research 22 (1): 31-45. doi: 10.1016/0033-5894(84)90004-8

Yaltırak C (1995). Gaziköy - Mürefte (Tekirdağ) arasının sedimanter ve tektonik özellikleri (in Turkish). TPJD Bülteni 6 (1): 93-112.

Yaltırak C (1996). Ganos Fay Sistemi'nin tektonik tarihi (in Turkish). TPJD Bülteni 8(1):137-156.

Yolsal- Çevikbilen S, Taymaz T (2012). Earthquake source parameters along the Hellenic subduction zone and numerical simulations of historical tsunamis in the Eastern Mediterranean. Tectonophysics 536–537: 61–100. doi: 10.1016/ j.tecto. 2012.02. 019